

A gut sense for a microbial pattern regulates feeding

<https://doi.org/10.1038/s41586-025-09301-7>

Received: 8 March 2023

Accepted: 16 June 2025

Published online: 23 July 2025

Open access

 Check for updates

Winston W. Liu^{1,2,3,20,21}, Naama Reicher^{1,3,21}, Emily Alway^{1,2,3,21}, Laura E. Rupprecht^{1,3}, Peter Weng^{1,2,3}, Chloe Schaeffen^{1,4}, Marguerita E. Klein^{1,2,3}, Jorge A. Villalobos^{1,3}, Carlos Puerto-Hernandez^{1,3}, Yolanda Graciela Kiesling Altún^{1,3}, Amanda Carbajal^{1,3}, José Alfredo Aguayo-Guerrero^{1,3,5}, Alam Coss^{1,3}, Atharva Sahasrabudhe^{6,7}, Polina Anikeeva^{6,7,8,9}, Alan de Araujo^{10,11}, Avnika Bali^{10,11}, Guillaume de Lartigue^{10,11}, Elvi Gil-Lievana^{12,13}, Ranier Gutierrez^{12,13}, Edward A. Miao^{14,15,16,17}, John F. Rawls^{3,15,17}, M. Maya Kaelberer^{1,2,3,18,22} & Diego V. Bohórquez^{1,2,3,16,17,19,22}

To coexist with its resident microorganisms, the host must have a sense to adjust its behaviour in response to them. In the intestine, a sense for nutrients transduced to the brain through neuroepithelial circuits guides appetitive choices^{1–5}. However, a sense that allows the host to respond in real time to stimuli arising from resident gut microorganisms remains to be uncovered. Here we show that in the mouse colon, the ubiquitous microbial pattern flagellin—a unifying feature across phyla⁶—stimulates Toll-like receptor 5 (TLR5) in peptide YY (PYY)-labelled colonic neuropod cells. This stimulation leads to PYY release onto NPY2R vagal nodose neurons to regulate feeding. Mice lacking TLR5 in these cells eat more and gain more weight than controls. We found that flagellin does not act on the nerve directly. Instead, flagellin stimulates neuropod cells from the colonic lumen to reduce feeding through a gut–brain sensory neural circuit. Moreover, flagellin reduces feeding independent of immune responses, metabolic changes or the presence of gut microbiota. This sense enables the host to adjust its behaviour in response to a molecular pattern from its resident microorganisms. We call this sense at the interface of the biota and the brain the neurobiotic sense⁷.

Every organism interprets the world through its senses—its Umwelt^{8,9}. Although five canonical senses have been extensively studied, emerging evidence has established the neural basis of a gut sense, a sense that constantly assesses stimuli arising from the gut lumen^{1–5,10–12}. Nutrients, stretch, and microorganisms are among the most salient stimuli that the gut encounters. In the small intestine, epithelial neuropod cells^{1,13–15} rapidly detect nutrients and relay the sensory information, through the vagus nerve, to influence an animal's appetitive choices in real time^{4,16–19}. Growing evidence suggests that gut microorganisms, which are most abundant in the colon²⁰, substantially modulate feeding behaviour^{21–24}, potentially through neuromodulators^{25–27}, immune signals²⁸ and vagal pathways^{23,24,29–34}. However, a direct neural circuit through which the host interprets microbial sensory information to adjust its feeding remains unknown.

In the colon, vagal neurons form neuroepithelial circuits with neuropod cells, labelled by the neuromodulator PYY^{1,3}. These, and other colonic epithelial cells, are constantly exposed to microorganisms, which can be recognized by molecular patterns such as flagellin,

collectively known as microbe-associated molecular patterns. Flagellin is a structural component of one of the three most ancient organelles, flagella³⁵, and a protein conserved across bacterial phyla⁶ that activates the pattern recognition receptor TLR5 (refs. 36,37). Deleting *Tlr5* in all intestinal epithelial cells of mice leads to obesity, metabolic inflammation, and spontaneous colitis²⁸. Furthermore, evidence from immortalized gut cell lines suggests that Toll-like receptors may be expressed by specialized sensory epithelial cells, including those that secrete the satiety-inducing protein PYY³⁸. Here we determined that feeding behaviour is regulated by a previously unrecognized gut–brain sensory modality for microbial patterns. We call this sense, at the interface of the biota and the brain, the neurobiotic sense.

PYY cells express *Tlr5*

In the gut, sensory epithelial cells are dispersed among other epithelial cells at a ratio of less than 1 in 1,000 (ref. 39). They encompass two main lineages: those that express serotonin and substance P, and those that

¹Laboratory of Gut Brain Neurobiology, Duke University, Durham, NC, USA. ²Department of Neurobiology, Duke University, Durham, NC, USA. ³Department of Medicine, Duke University, Durham, NC, USA. ⁴Trinity College of Arts & Sciences, Duke University, Durham, NC, USA. ⁵Laboratory of Immunometabolism, Research Division, General Hospital of Mexico Dr. Eduardo Liceaga, Mexico City, Mexico. ⁶Research Laboratory of Electronics, Massachusetts Institute of Technology, Cambridge, MA, USA. ⁷McGovern Institute for Brain Research, Massachusetts Institute of Technology, Cambridge, MA, USA. ⁸Department of Materials Science and Engineering, Massachusetts Institute of Technology, Cambridge, MA, USA. ⁹Department of Brain and Cognitive Sciences, Massachusetts Institute of Technology, Cambridge, MA, USA. ¹⁰Monell Chemical Senses Center, Philadelphia, PA, USA. ¹¹Department of Neuroscience, Perelman School of Medicine, University of Pennsylvania, Philadelphia, PA, USA. ¹²Laboratory Neurobiology of Appetite, Department of Pharmacology, CINVESTAV, Mexico City, Mexico. ¹³Center for Research on Aging (CIE), CINVESTAV Sede Sur, Mexico City, Mexico. ¹⁴Department of Integrative Immunobiology, Duke University, Durham, NC, USA. ¹⁵Department of Molecular Genetics and Microbiology, Duke University, Durham, NC, USA. ¹⁶Department of Pathology, Duke University, Durham, NC, USA. ¹⁷Department of Cell Biology, Duke University, Durham, NC, USA. ¹⁸Department of Physiology, University of Arizona, Tucson, AZ, USA. ¹⁹Duke Institute for Brain Sciences, Duke University, Durham, NC, USA. ²⁰Present address: Department of Dermatology, Stanford University School of Medicine, Redwood City, CA, USA. ²¹These authors contributed equally: Winston W. Liu, Naama Reicher, Emily Alway. ²²These authors jointly supervised this work: M. Maya Kaelberer, Diego V. Bohórquez.

[✉]e-mail: mkaelberer@arizona.edu; diego.bohorquez@duke.edu

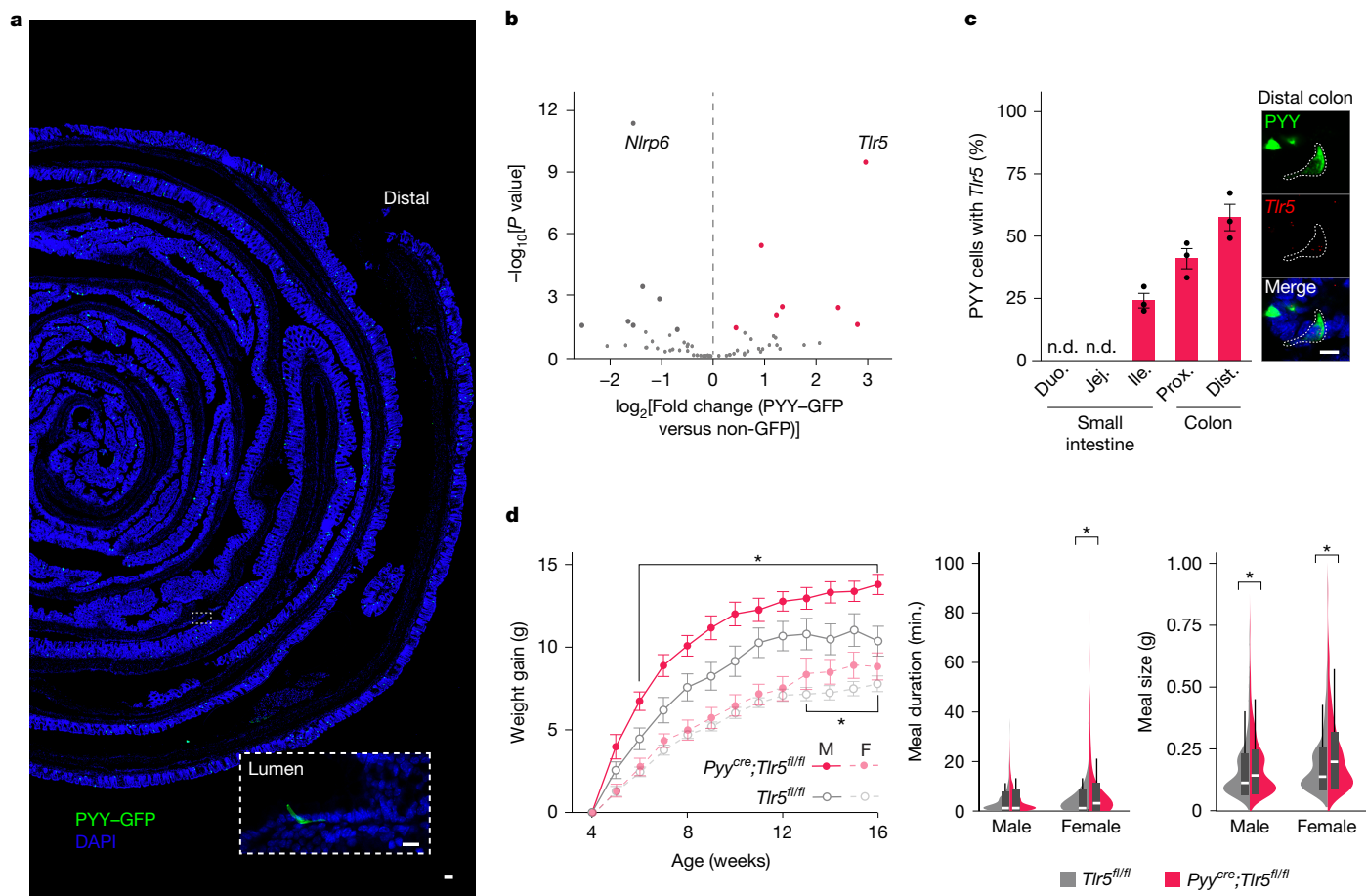


Fig. 1 | The absence of microbial pattern recognition receptor TLR5 in colonic PYY-labelled cells increases food intake. **a**, Mouse colon with GFP-labelled PYY-labelled cells was rolled longitudinally (proximal colon in the centre); representative of $n = 3$ mice. Inset: magnified view of the outlined area showing a single PYY-GFP cell with apical process reaching into the lumen and neuropod reaching towards the base of the crypt. DAPI, 4',6-diamidino-2-phenylindole. Scale bars, 10 μm . **b**, Volcano plot of microbial pattern recognition receptor gene expression in epithelial PYY-GFP and non-GFP cells by RNA sequencing. Compared to non-GFP cells, PYY-GFP cells are enriched for the pattern recognition receptor gene *Tlr5* ($n = 6$ mice; adjusted $P < 0.01$ by DESeq2 with two-tailed t -test). **c**, Fluorescence in situ hybridization of *Tlr5* in PYY-GFP cells. Error bars represent s.e.m. Left: regional expression of *Tlr5* in PYY-GFP cells ($n = 3$ mice, each dot represents 50 cells). n.d., not detected (no cells expressing *Tlr5*). Dist. distal; Duo., duodenum; Jej., jejunum; Ile., ileum; Prox., proximal. Right, PYY-labelled cell (green) expressing *Tlr5* (red) in the distal colon; representative of $n = 3$ mice. Scale bar, 10 μm . White dashed line represents PYY-labelled cell outline. **d**, Left, genetic deletion of *Tlr5* exclusively

in PYY-labelled cells causes increased weight gain in male and female mice (males (M) *Pyy^{cre};Tlr5^{fl/fl}*; $n = 7$ mice, starting weight = 5.78 ± 0.61 ; *Tlr5^{fl/fl}* littermate controls: $n = 15$ mice, starting weight = 14.28 ± 0.71 ; females (F) *Pyy^{cre};Tlr5^{fl/fl}*; $n = 6$ mice, starting weight = 15.04 ± 0.53 ; *Tlr5^{fl/fl}* littermate controls: $n = 11$ mice, starting weight = 14.16 ± 0.39 ; $*P < 0.05$ genotype-time interaction by repeated-measures analysis of variance (ANOVA) with post hoc Tukey honestly significant difference (HSD). Error bars represent s.e.m. Right, meal duration in females and meal size in males and females significantly increased in *Pyy^{cre};Tlr5^{fl/fl}* mice (*Tlr5^{fl/fl}* males: $n = 413$ meals, $n = 6$ mice; *5Pyy^{cre};Tlr5^{fl/fl}* males: $n = 612$ meals, $n = 9$ mice; *Tlr5^{fl/fl}* females: $n = 399$ meals, $n = 8$ mice; *Pyy^{cre};Tlr5^{fl/fl}* females: $n = 468$ meals, $n = 9$ mice; $n = 2$ independent experiments; $*P < 0.05$ by two-way ANOVA with post hoc Tukey HSD; $P < 0.05$ main effect of genotype and sex for meal size and duration with $P > 0.05$ genotype-sex interaction). No changes observed in meal frequency (see Extended Data Fig. 5 for further analyses). Box plots represent interquartile range; white lines indicate median; whiskers extend to the furthest point above the third quartile or below the first quartile within $1.5 \times$ the interquartile range.

express several neuromodulators including cholecystokinin (CCK), glucagon-like peptide 1 (GLP-1) and PYY^{40,41}. The expression of these neuropeptides is preceded by that of the transcription factor *Neurod1* (ref. 42). In different regions of the intestine, *Neurod1*-labelled cells favour the expression of specific neuromodulators. For example, CCK prevails in the proximal small intestine, whereas PYY is enriched in the distal ileum and colon^{13,39} (Fig. 1a). The colon is a habitat rich in microorganisms²⁰. Using reporter mice expressing green fluorescent protein (GFP) driven by the CCK and PYY promoters, we sequenced the transcriptome of epithelial cells from the small intestine and colon (Extended Data Fig. 1). In each segment, we compared the transcriptome of sensory epithelial cells to that of their neighbouring epithelial cells to identify enriched receptors that detect microbial signals, including byproducts of dietary fermentation, metabolites, and patterns^{23,27,28}.

Both CCK-GFP cells in the proximal small intestine and PYY-GFP cells in the ileum and colon were significantly enriched in genes encoding receptors of microbial byproducts, such as *Ffar1*, *Ffar2*, *Gpbar1* and *Gpr119* ($n \geq 5$ mice, $P < 0.001$; Extended Data Fig. 1). However, only PYY-GFP cells were significantly enriched in genes for pattern recognition receptors, the most prominent being *Tlr5* ($n = 6$ mice, $P < 0.01$; Fig. 1b). TLR5 detects flagellin^{36,37}, a ubiquitous microbial pattern, classically associated with host immune defence and commensal tolerance⁴³⁻⁴⁵.

The robust expression of *Tlr5* in PYY-labelled cells was corroborated using in situ hybridization. Overall, co-localization significantly increased from $24.1 \pm 2.9\%$ in the ileum to $57.5 \pm 5.3\%$ in the distal colon ($n = 3$ mice, 50 cells per segment; $P < 0.005$, Fig. 1c), where PYY-labelled cell density is highest ($n = 3$; Extended Data Fig. 2a). *Tlr5* was not expressed in PYY-labelled cells of the brain⁴⁶ or serotonin-labelled cells of the colon; in fact, *Tlr5* was predominantly expressed in

PYY-labelled cells of the ileum and colon ($n = 3$ mice; Extended Data Fig. 2b–h).

TLR5 in PYY cells regulates feeding

To determine the role of TLR5 in PYY-labelled cells, we bred *Pyy^{cre};Tlr5^{fl/fl}* mice. In these mice, *Tlr5* is knocked out of all PYY-labelled cells ($n = 3$ mice; Extended Data Fig. 3a). Studies have shown that a global knockout of *Tlr5* in mice causes metabolic dysfunction, inflammation, and obesity²¹. Furthermore, when TLR5 is ablated in all gut epithelial cells, both the metabolic dysfunction and inflammation persist²⁸. However, we found that when TLR5 is ablated specifically in PYY-labelled cells, mice show no evidence of metabolic dysfunction or inflammation (Extended Data Fig. 3).

Compared to littermate controls, *Pyy^{cre};Tlr5^{fl/fl}* mice had normal oral glucose tolerance, fasting blood glucose ($n \geq 4$ mice, $P > 0.1$; Extended Data Fig. 3b,c), and fat pad weight ($n \geq 5$ mice, $P > 0.1$, Extended Data Fig. 3d). *Pyy^{cre};Tlr5^{fl/fl}* mice also showed no change in the serum levels of the metabolic neuromodulators GLP-1 and PYY following 1 h of food consumption, suggesting that the circulating levels of gut hormones were no different from those of littermate controls ($n \geq 5$ mice, $P > 0.1$; Extended Data Fig. 3e). Moreover, these mice showed no signs of spontaneous colitis and exhibited normal colon length, weight and spleen size ($n \geq 3$ mice, $P > 0.1$; Extended Data Fig. 3f–h). Levels of the inflammatory markers colonic myeloperoxidase and fecal lipocalin-2 were unchanged between *Pyy^{cre};Tlr5^{fl/fl}* mice and controls ($n \geq 5$ mice, $P > 0.1$; Extended Data Fig. 3i). Furthermore, there were no histological differences in the colon, including crypt depth and sensory cell density ($n = 3$ mice, $P > 0.05$; Extended Data Fig. 3j–l), TLR gene expression in epithelial cells remained unaltered ($n = 6$ mice, $P > 0.05$; Extended Data Fig. 3m), and no changes in tight junctions were observed ($n = 6$ mice, $P > 0.05$; Extended Data Fig. 3n) in *Pyy^{cre};Tlr5^{fl/fl}* mice compared to littermate controls.

Notably, when TLR5 is ablated specifically in PYY-labelled cells, mice eat more and gain more weight ($n \geq 4$ mice, $P < 0.05$; Fig. 1d, Extended Data Fig. 3o–p and Supplementary Table 1). As TLR5 is known to canonically trigger immune responses through intracellular activation of myeloid differentiation factor 88 (MyD88)⁴⁷, we bred *Pyy^{cre};Myd88^{fl/fl}* mice to determine the effect of MyD88 ablation in PYY-labelled cells. We found that, compared to littermates, *Pyy^{cre};Myd88^{fl/fl}* mice did not show increased body weight gain or food intake ($n \geq 3$ mice, $P > 0.1$; Extended Data Fig. 4). Therefore, independent of canonical immune signalling, metabolic dysfunction, or inflammation, TLR5 in PYY-labelled cells regulates body weight gain.

Furthermore, we performed meal pattern analysis to determine the quantity, frequency, and timing of food ingestion. We optimized an automated home-cage behavioural system that records food intake to the nearest 0.01 g with temporal resolution of 1 s (Extended Data Fig. 5a). Both male and female *Pyy^{cre};Tlr5^{fl/fl}* mice ate significantly larger meals compared to littermate controls (males: $n = 6$ –9 mice; females: $n = 8$ –9 mice; $P < 0.05$; Fig. 1d and Extended Data Fig. 5b,c). Moreover, female *Pyy^{cre};Tlr5^{fl/fl}* mice also ate longer meals than littermate controls ($n = 8$ –9, $P < 0.05$; Fig. 1d and Extended Data Fig. 5d–g), revealing that the length and size of meals are modulated by TLR5 in PYY-labelled cells.

PYY cells use TLR5 to sense flagellin

The established ligand for TLR5 is flagellin. Although transcriptional models suggest that diet influences microbial signals⁴⁸, it is unclear whether the amount of colonic flagellin changes with feeding. Using a cell-based assay, we found that relative flagellin levels in the stool are significantly higher in fed compared to fasted mice ($n = 5$, mice $P < 0.05$; Fig. 2a). This response is unaltered in *Pyy^{cre};Tlr5^{fl/fl}* mice ($n = 5$ mice,

$P > 0.1$; Fig. 2a), indicating that flagellin levels in the colon are independent of *Tlr5* expression in PYY-labelled cells. Thus, feeding correlates with increased flagellin in the colon.

Analysis by quantitative reverse transcription PCR (qRT-PCR) confirmed expression of *Tlr1–Tlr5* in colonic PYY-GFP cells; however, compared to the expression levels in neighbouring epithelial cells, only *Tlr5* expression showed significant enrichment in PYY-labelled cells ($n \geq 5$ mice, $P < 0.05$; Fig. 2b). To determine whether these cells respond to ligands for Toll-like receptors, we recorded intracellular calcium activity from colonic PYY-labelled cells. We bred a *Pyy^{cre};Salsa6f* mouse in which PYY-labelled cells express the SALSA6F protein. This fusion protein, linking tdTomato and GCaMP6f, allows for sorting primary cells on the basis of their red fluorescence, and recording their intracellular calcium activity while avoiding the toxicity of calcium indicator dyes⁴⁹.

Of all *Pyy^{cre};Salsa6f* cells imaged, none responded to the TLR4 ligand lipopolysaccharide (1 mg ml^{-1} , $n = 80$ cells from 3 mice; Fig. 2c), 19% responded to the TLR3 ligand poly(I:C) ($1 \mu\text{g ml}^{-1}$, $n = 63$ cells from 4 mice; Fig. 2c) and 26% responded to the TLR5 ligand flagellin (100 ng ml^{-1} , $n = 121$ cells from 5 mice; Fig. 2c). The calcium responses to poly(I:C) were unaltered in the presence of the TLR5 inhibitor TH1020 ($n = 12$ cells from 3 mice, $P > 0.5$; Fig. 2d,e), but the responses to flagellin were significantly attenuated ($n = 9$ cells from 3 mice, $P < 0.05$; Fig. 2d,e), demonstrating that flagellin activation of PYY-labelled cells requires TLR5. Similar results were confirmed using NeuroD1-Cre;Salsa6f mice (Extended Data Fig. 6a,b).

We then determined whether the activation of PYY-labelled cells by TLR ligands leads to the release of PYY. Although poly(I:C) ($1 \mu\text{g ml}^{-1}$) did not stimulate PYY release from dissociated colonic crypts compared to buffer ($n \geq 5$ mice, $P < 0.01$; Extended Data Fig. 6c), flagellin (100 ng ml^{-1}) stimulated significant release of PYY ($n = 5$ mice, $P < 0.05$; Extended Data Fig. 6c). This release was significantly suppressed in colonic crypts from mice lacking TLR5 in PYY-labelled cells ($n = 4$ mice, $P < 0.05$; Fig. 2f). Therefore, PYY-labelled cells sense flagellin using TLR5 and transduce it by releasing PYY—a known inducer of satiety⁵⁰.

PYY cells connect with vagal neurons

Besides the circulatory functions of intestinal PYY^{50,51}, recent work shows local paracrine and synaptic signalling onto the vagus nerve^{52,53}. Previously, monosynaptic rabies tracing has shown that PYY-labelled cells in the colon form synaptic connections with vagal neurons. These cells, known as neuropod cells, rapidly and directly transduce sensory cues to the nervous system^{3,54}.

Compared to neighbouring epithelial cells, PYY-labelled cells are significantly enriched in genes encoding proteins involved in synaptic signalling, synaptic formation and neurotransmission ($n = 6$ mice, $P < 0.01$; Fig. 2g and Extended Data Fig. 7a,b). In addition, approximately one in five PYY-labelled cells contact peripheral neurons labelled by PGP9.5 in the ileum and colon ($21.7 \pm 0.6\%$, $n = 50$ cells per segment; Fig. 2h and Extended Data Fig. 7c). To confirm that PYY-labelled cells are functionally connected with the vagus nerve, we paired luminal optogenetics with *in vivo* whole-nerve electrophysiology of the cervical vagus nerve. We bred a *Pyy^{cre};ChR2* mouse in which PYY-labelled cells express channelrhodopsin-2 (ChR2), which is an opsin activated by 473-nm light (Extended Data Fig. 7d,e). In *Pyy^{cre};ChR2* mice, a control 532-nm-light stimulus applied to the lumen of the colon did not activate the cervical vagus, but a 473-nm-light luminal stimulus led to a rapid and significant increase in the vagal firing rate ($n = 3$ mice, $P < 0.05$; Fig. 2i). Vagal firing peaked within seconds of 473-nm-light stimulus, demonstrating that PYY-labelled cells directly activate the vagus nerve. These results establish a direct PYY-labelled cell–vagal circuit for rapid signalling between the colon and the hindbrain, where the afferent vagus nerve terminates⁵⁵.

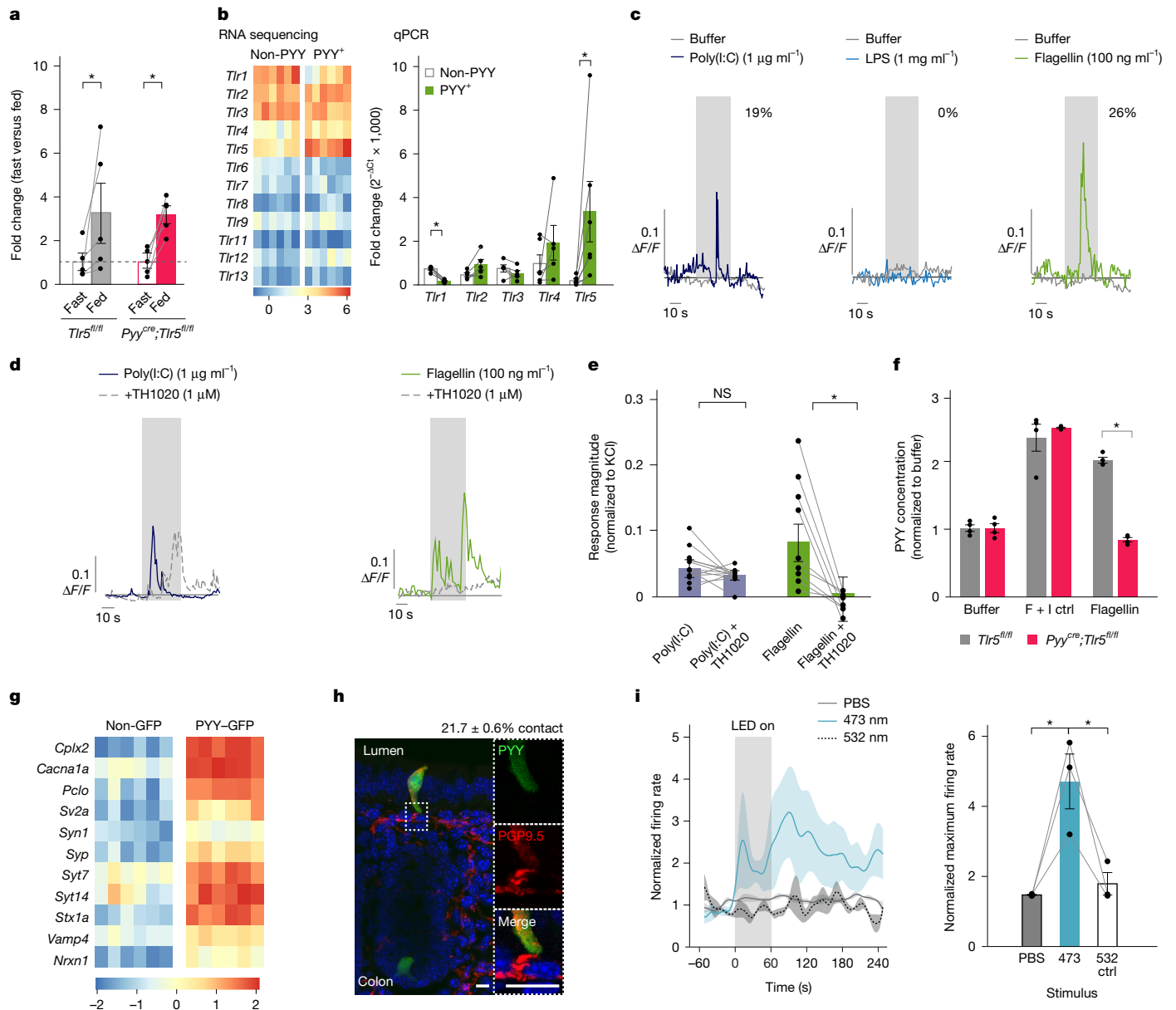


Fig. 2 | PYY-labelled cells sense microbial flagellin through TLR5. **a**, Relative stool flagellin concentration from *Pyy^{cre};Tlr5^{fl/fl}* mice and *Tlr5^{fl/fl}* littermate controls following 16-h fast or ad libitum feeding. No differences across genotype. Feeding increased stool flagellin ($n = 5$ mice; $*P < 0.05$ by repeated-measures ANOVA with post hoc two-tailed Tukey HSD). **b**, Heat map ($n = 6$ mice; adjusted $*P < 0.01$ by DESeq2 with two-tailed t -tests; P values in Extended Data Fig. 1; left) and qRT-PCR (non-PYY, $n = 5$ mice; PYY, $n = 6$ mice; $*P < 0.05$ by repeated-measures ANOVA with post hoc Tukey HSD; right) of TLR gene expression in non-GFP and PYY-GFP colonic epithelial cells. **c**, Selected calcium responses of *Pyy^{cre};Salsa6f* colonic cells to poly(I:C) (19%, $n = 63$ cells, $n = 4$ mice), lipopolysaccharide (LPS; 0%, $n = 80$ cells, $n = 3$ mice) and flagellin (26%, $n = 121$ cells, $n = 5$). Grey bar indicates 30-s infusion. **d**, Calcium responses to poly(I:C) and flagellin before (solid) and after (dashed) TLR5 inhibitor TH1020 (1 μM). **e**, Calcium response quantification. Only flagellin, not poly(I:C), responses were reduced (poly(I:C): $n = 12$ cells; flagellin: $n = 9$ cells; $*P < 0.05$ by paired,

two-tailed t -test). NS, not significant. **f**, Colonic epithelial monolayer cultures from *Pyy^{cre};Tlr5^{fl/fl}* mice and *Tlr5^{fl/fl}* littermate controls stimulated with buffer, 100 ng ml^{-1} flagellin and 1 μM forskolin (F) + 10 μM IBMX (I; positive control (ctrl)). PYY concentration in cell lysates and supernatants measured using enzyme-linked immunosorbent assay. Flagellin stimulated PYY release in *Tlr5^{fl/fl}* but not *Pyy^{cre};Tlr5^{fl/fl}* cultures ($n = 4$ mice; $*P < 0.05$ by repeated-measures ANOVA with post hoc two-tailed Tukey HSD). **g**, Heat map of synaptic gene expression in non-GFP and PYY-GFP colonic cells ($n = 6$ mice; adjusted $P < 0.01$ by DESeq2 with two-tailed t -tests; P values in Extended Data Fig. 1). **h**, Colonic PYY-GFP tissue immunostained for PGP9.5 (red). Representative of $n = 3$ mice; regions quantified in Extended Data Fig. 7. Scale bars, 10 μm . **i**, Left: vagal responses to intracolonic PBS and stimulation by a 473-nm and 532-nm light-emitting diode (LED) in *Pyy^{cre};ChR2* mice ($n = 3$ mice). Right: quantification of peak vagal responses ($n = 3$ mice; $*P < 0.05$ by two-tailed Wilcoxon signed ranked test with non-parametric comparisons). Error bars and shading represent s.e.m.

Flagellin is transduced to vagal neurons

We then recorded cervical vagal activity in response to colonic perfusion of flagellin. Intralipid served as a positive control ($n = 4$ mice, $P < 0.05$; Extended Data Fig. 7f,g). Perfusing flagellin (2 $\mu\text{g ml}^{-1}$) through the colon resulted in a significant increase in vagal firing rate within

seconds ($n = 7$ mice, $P < 0.05$; Fig. 3a). To determine whether the PYY-labelled cell is necessary to transduce luminal flagellin onto the vagus, we bred a *Pyy^{cre};Halo* mouse. In these mice, PYY-labelled cells express the optogenetic silencing protein halorhodopsin (Extended Data Fig. 7h), an anion channel that hyperpolarizes cells in response to 532-nm light. A control 473-nm-light stimulus applied to the

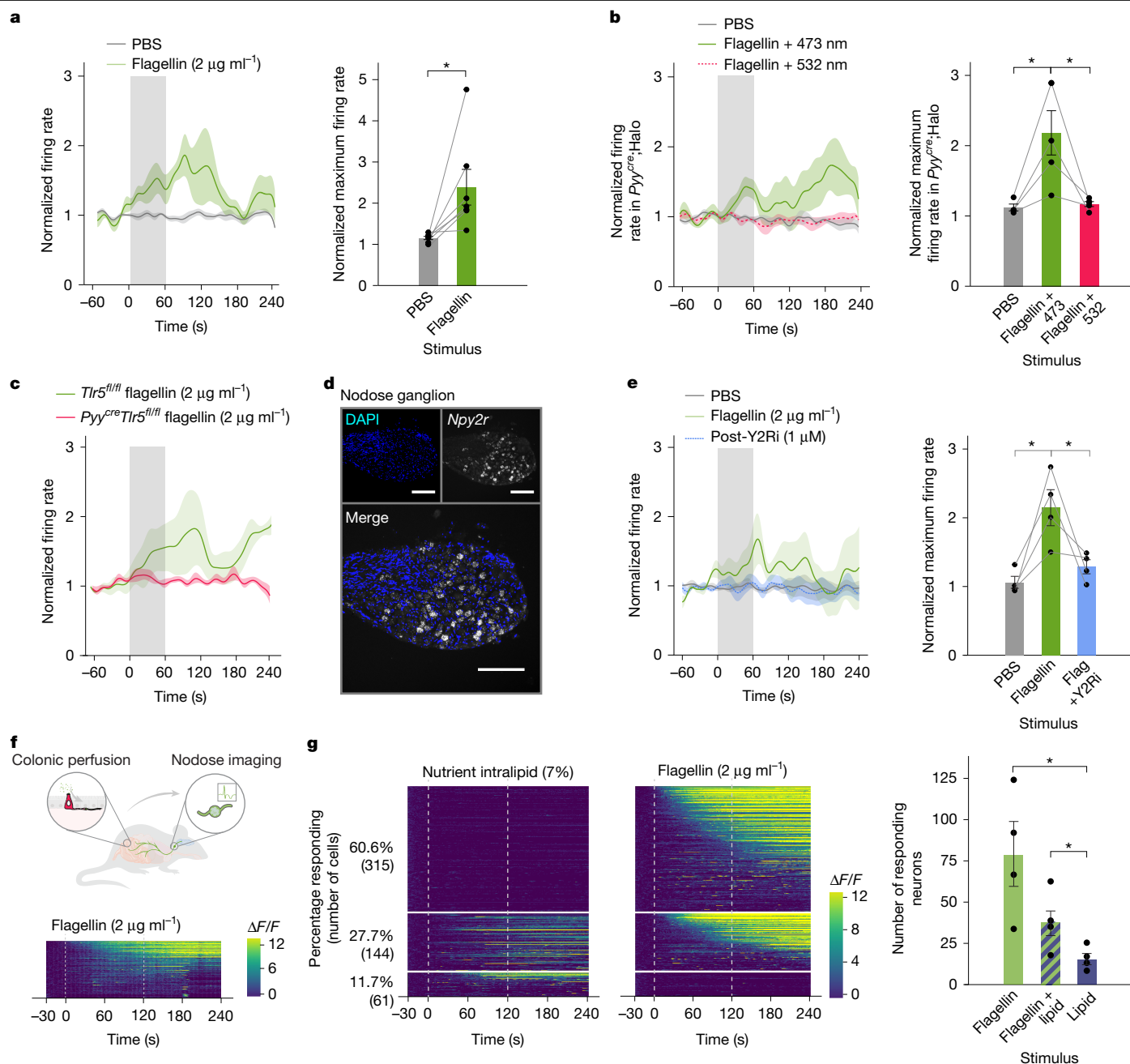


Fig. 3 | PYY-vagal circuits transduce colonic flagellin. **a**, Left, vagal responses to intracolonic perfusion of PBS or $2 \mu\text{g ml}^{-1}$ flagellin in wild-type mice ($n = 7$ mice). Right, quantification of peak response to flagellin ($n = 7$ mice; $*P < 0.05$ by two-tailed paired t -test). **b**, Left, vagal responses to intracolonic perfusion of PBS and $2 \mu\text{g ml}^{-1}$ flagellin with simultaneous 473-nm-LED or 532-nm-LED stimulation in $\text{Pyy}^{\text{cre}};\text{Halo}$ mice ($n = 4$ mice). Right, quantification of the peak vagal response to flagellin ($n = 4$ mice; $*P < 0.05$ by two-tailed Wilcoxon signed ranked test with non-parametric comparisons using the Wilcoxon method). **c**, Vagal responses to intracolonic perfusion of flagellin in $\text{Pyy}^{\text{cre}};\text{Tlr5}^{\text{fl/fl}}$ mice ($n = 5$ mice) and $\text{Tlr5}^{\text{fl/fl}}$ littermate controls ($n = 3$ mice; for quantification, see Extended Data Fig. 8). **d**, Fluorescence in situ hybridization of PYY receptor Y2R (encoded by *Npy2r*) in a subpopulation of neurons in the vagal nodose ganglion. Representative of $n = 4$ ganglia. Scale bars, $10 \mu\text{m}$. **e**, Left, vagal responses to intracolonic perfusion of PBS or $2 \mu\text{g ml}^{-1}$ flagellin before and

after intraperitoneal delivery of the Y2R inhibitor (Y2Ri) BIIE-0246 ($1 \mu\text{M}$; $n = 4$ mice). Right, quantification of the peak vagal response to flagellin with and without the addition of Y2R inhibitor $1 \mu\text{M}$ BIIE-0246 ($n = 4$ mice; $*P < 0.05$ by Kruskal–Wallis test with non-parametric comparisons using the Wilcoxon method). **f**, In vivo calcium imaging of vagal nodose neurons positive for *Npy2r* in response to colonic perfusion of flagellin ($2 \mu\text{g ml}^{-1}$; $n = 4$ mice, $n = 144$ neurons). A total of 43.37% of NPY2R^+ cells respond to $2 \mu\text{g ml}^{-1}$ flagellin. **g**, Left, in vivo calcium imaging of vagal nodose neurons in response to colonic perfusion of either intralipid (7%) or flagellin ($2 \mu\text{g ml}^{-1}$). $n = 520$ neurons, $n = 4$ mice. Right, number of responding neurons to each stimulus ($n = 4$ mice, $n = 520$ neurons). Grey dashed lines in the heat maps represent start and end of perfusion. Error bars and shading represent s.e.m. Graphics in **f** adapted with permission from ref. 3, AAAS.

lumen of the colon did not alter vagal activity in response to flagellin ($2 \mu\text{g ml}^{-1}$), but a silencing 532-nm-light luminal stimulus ablated vagal firing in response to flagellin ($n = 4$ mice, $P < 0.05$; Fig. 3b). Moreover, in $\text{Pyy}^{\text{cre}};\text{Tlr5}^{\text{fl/fl}}$ mice, luminal flagellin produced no rapid vagal response

compared to the case in littermate controls ($n \geq 3$ mice, $P < 0.05$; Fig. 3c and Extended Data Fig. 8a). Therefore, PYY-labelled neuropod cells use TLR5 to sense luminal flagellin and rapidly transduce this microbial stimulus to the vagus nerve.

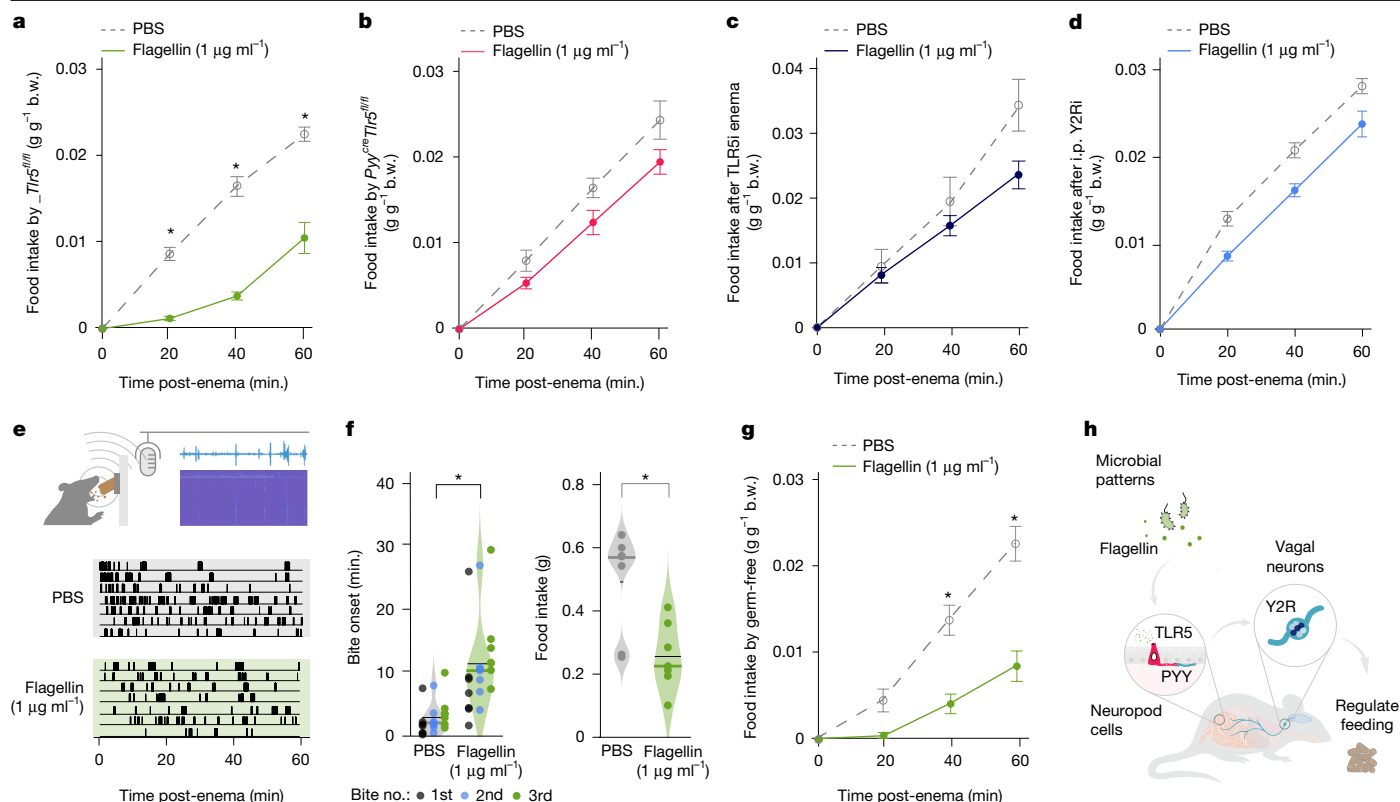


Fig. 4 | PYY-vagal circuits use TLR5 and Y2R to drive changes in food intake. Mice were fasted overnight and given an enema of either 1 μg ml⁻¹ flagellin or PBS before receiving access to standard chow ad libitum. **a, b**, *Tlr5^{fl/fl}* littermate control mice ate significantly less food post-flagellin enema at 20, 40 and 60 min (**a**), whereas *Pyy^{cre}Tlr5^{fl/fl}* mice did not (**b**; $n = 5$ mice per genotype; $*P < 0.05$ genotype-enema-time interaction by repeated-measures ANOVA with post hoc two-tailed Tukey HSD). **c, d**, In wild-type mice, PBS and flagellin enemas were performed with the addition of either 10 μM TH1020 in the enema solution ($n = 8$ mice; **c**) or intraperitoneal injection of 1 μM BIIE-0246 before enema ($n = 10$ mice; **d**). TLR5 and Y2R inhibition attenuated the reduction of food intake post-flagellin enema ($P < 0.05$ drug-enema-time interaction by repeated-measures ANOVA with post hoc Tukey HSD; see Extended Data Fig. 9c, d for vehicle controls). i.p., intraperitoneal. **e**, Crunch Master (top schematic) tracks feeding microstructure by means of audio and video recording. Black ticks

(bottom) indicate biting patterns of $n = 7$ mice post-PBS or flagellin enema. **f**, Left, flagellin enema significantly delayed onset of the first three bites (black: bite 1; blue: bite 2; green: bite 3; $*P < 0.0001$ main effect of treatment by repeated-measures ANOVA). Right, intake (spillage-corrected) was significantly decreased over 1-h test session after flagellin enema (two-tailed unpaired t -test, $*P < 0.01$). Violin plots show median indicated by thick line and mean indicated by thin line. **g**, In wild-type germ-free mice, flagellin enema decreased food intake compared to PBS enema ($n = 12$ mice; $*P < 0.05$, enema-time interaction by repeated-measures ANOVA with post hoc two-tailed Tukey HSD). Error bars represent s.e.m. **h**, Model for microbial pattern sensing by neuroepithelial circuits to drive behavioural change. Bacterial flagellin is detected by TLR5 in colonic PYY-labelled cells, which in turn release PYY to activate vagal neurons through Y2R. Activation of this circuit contributes to overall food intake. Graphics in **h** adapted with permission from ref. 3, AAAS.

Notably, molecular analyses using RNA sequencing, qRT-PCR and in situ hybridization show that vagal neurons do not express *Tlr5* ($n \geq 3$ mice; Extended Data Fig. 8b–d). Moreover, calcium imaging of acutely dissociated vagal nodose neurons revealed that whereas capsaicin (the control stimulus) elicits calcium transients, flagellin does not, indicating that vagal nodose neurons themselves do not sense flagellin ($n = 227$ neurons from 4 mice; Extended Data Fig. 8e), further establishing PYY-labelled neuropod cells as flagellin transducers.

Vagal NPY2 receptor is required

We then sought to determine whether vagal activity in response to flagellin requires PYY release from neuropod cells. Published RNA-sequencing data show that vagal neurons innervating the colon express the PYY receptor Y2R⁵⁶ ($n = 44$ cells; Extended Data Fig. 8f). In the gut, this receptor is thought to mediate local PYY signalling⁵¹. Using in situ hybridization, we confirmed the expression of Y2R in vagal nodose neurons ($n = 4$ mice; Fig. 3d). Then, we found that blocking Y2R using BIIE-0246 (10 μM) ablates cervical vagal activity in response to flagellin perfused through the lumen of the colon ($n = 4$ mice, $P < 0.05$; Fig. 3e).

To better understand how individual vagal neurons respond to flagellin in the gut, we used intravital calcium imaging to observe the activity of these neurons in response to stimuli perfused through the colon. We used a triple-transgenic mouse model, Snap25-FosTRAP-tdTomato^{57,58}, that enables real-time tracking of calcium changes in individual vagal neurons and subsequent labelling of these responsive neurons for further analysis. After imaging, we extracted the nodose ganglia and using compartment analysis of temporal activity by fluorescence in situ hybridization⁵⁹, we confirmed that 43.37% of 332 NPY2R-labelled neurons reacted to flagellin in the colon (Fig. 3f and Extended Data Fig. 8g–i).

Moreover, calcium imaging of vagal nodose neurons revealed distinct response patterns: 11.7% of neurons responded only to intralipid (a positive control), 27.7% responded to both intralipid and flagellin, and 60.6% responded exclusively to flagellin ($n = 520$ neurons; $n = 4$ mice; Fig. 3g and Extended Data Fig. 8j). This observation—that almost two thirds of the neurons activated by colonic infusions specifically responded to flagellin—suggests the existence of a unique neuroepithelial circuit for sensing flagellin, separate from the pathways involved in nutrient detection. Although future studies should investigate the neurons responding to both intralipid and flagellin, these results highlight a

distinct pathway for gut–brain signalling in response to the microbial pattern flagellin.

Flagellin regulates feeding through PYY cells

Our discovery of a neuroepithelial circuit for rapid sensing of a microbial pattern in the colon led us to investigate how flagellin influences behaviour in real time. We reasoned that the presence of flagellin in the colon would lead to a rapid decrease in food intake. To test this, we fasted mice overnight to induce hunger and then administered either flagellin ($1 \mu\text{g ml}^{-1}$, 0.1 ml) or a PBS control by means of enema. We found that a flagellin enema significantly reduced food intake within 20 min in littermate control mice but had no effect on mice lacking TLR5 in PYY-labelled cells (*Pyy^{cre}; Tlr5^{fl/fl}*; $n = 5$ mice, $P < 0.05$; Fig. 4a,b and Extended Data Fig. 9a). This response to flagellin was consistent across juvenile (5-week-old) and adult (10-week-old) mice, suggesting that this sensory pathway is conserved throughout development ($n = 5$ mice, $P < 0.05$; Extended Data Fig. 9b).

To examine the specificity of the flagellin effect, we conducted an enema containing poly(I:C), a TLR3 ligand, and found that this stimulus did not affect food intake ($n \geq 5$ mice, $P < 0.05$; Extended Data Fig. 9c). Furthermore, flagellin caused a temporary decrease in food intake, which dissipated after 3 h ($n = 5$ mice, $P < 0.05$; Extended Data Fig. 9c). Finally, pharmacologically inhibiting either TLR5 or the Y2 receptor prevented the flagellin-induced reduction in food intake ($n \geq 8$ mice, $P < 0.05$; Fig. 4c,d and Extended Data Fig. 9d,e). These data strongly suggest that luminal flagellin rapidly and reversibly suppresses food intake by acting on TLR5 and triggering the release of PYY within this neuroepithelial circuit.

To analyse feeding behaviour with greater precision, we developed a behavioural system using video and audio recordings. The system, referred to as Crunch Master, serves to automatically quantify individual bite bouts in real time (Fig. 4e and Supplementary Videos 1 and 2). This analysis revealed that a flagellin enema delayed the onset of feeding and reduced overall food consumption without affecting bite frequency or eating duration within a 1-h period ($n = 7$ mice per group, $P < 0.0001$; Fig. 4f and Extended Data Fig. 9e). This further demonstrates that colonic flagellin stimulation modulates feeding behaviour in real time.

Notably, levels of flagellin delivered by means of enema were within the range of physiological concentrations found in fed versus fasted mice ($n \geq 5$ mice, $P < 0.05$; Extended Data Fig. 9f). In addition, mice showed no signs of malaise, diarrhoea, pain, or physical limitations, and there was no significant increase in cytokine expression in the colon or spleen within 1 h post-enema ($n \geq 5$ mice, $P < 0.05$; Extended Data Fig. 10a,b). Thus, neuroepithelial sensing of flagellin reduces food intake in the absence of an immune response.

Finally, to confirm that the effects of flagellin on food intake were due to direct activation of epithelial cells, and not interactions with gut microorganisms, we administered a flagellin enema to germ-free mice. Although germ-free mice can exhibit behavioural variations compared to conventionally raised animals⁶⁰, they are a useful model for studying this gut–brain neural circuit without a microbiome. Our results show that a flagellin enema significantly reduced food intake in these germ-free mice within 1 h ($n = 12$ mice, $P < 0.05$; Fig. 4g). This demonstrates that direct sensing of flagellin by colonic epithelial cells is sufficient to suppress food intake, irrespective of other microbial signals. Collectively, these findings demonstrate that a gut sense for the microbial pattern flagellin regulates feeding (Fig. 4h).

Conclusion

This gut–brain neural circuit forms the foundation of a ‘neurobiotic sense’—a sense by which the host adjusts its behaviour by monitoring a gut microbial pattern. While previous research has focused on nutrient

sensory transduction in the small intestine^{4,16,17,19}, we discovered that the specialized colonic cells, PYY-labelled neuropod cells, utilize the pattern recognition receptor TLR5 to detect bacterial flagellin. These cells then rapidly signal to the brain, through the vagus nerve, to regulate feeding behaviour.

It is important to acknowledge that, in this study, one type of flagellin from *Salmonella typhimurium*, a stereotypical pathogen, was used. However, bacteria can be pathogenic or commensal depending on the specific flagellin variant expressed⁴⁵. Therefore, the effects of other molecular variants of flagellin warrant investigation. Future research should leverage developing technologies for real-time modulation of microbial populations to investigate the effects of flagellin fluctuations independently of exogenous induction.

Just as organisms rely on sight, sound, scent, taste and touch to navigate the world, they also adjust their behaviour in response to stimuli shaping their gut Umwelt⁷.


Online content

Any methods, additional references, Nature Portfolio reporting summaries, source data, extended data, supplementary information, acknowledgements, peer review information; details of author contributions and competing interests; and statements of data and code availability are available at <https://doi.org/10.1038/s41586-025-09301-7>.

1. Bohórquez, D. V. et al. Neuroepithelial circuit formed by innervation of sensory enteroendocrine cells. *J. Clin. Invest.* **125**, 782–786 (2015).
2. Bellono, N. W. et al. Enterochromaffin cells are gut chemosensors that couple to sensory neural pathways. *Cell* **170**, 185–198 (2017).
3. Kaelberer, M. M. et al. A gut–brain neural circuit for nutrient sensory transduction. *Science* **361**, eaat5236 (2018).
4. Buchanan, K. L. et al. The preference for sugar over sweetener depends on a gut sensor cell. *Nat. Neurosci.* **25**, 191–200 (2022).
5. Furness, J. B., Rivera, L. R., Cho, H. J., Bravo, D. M. & Callaghan, B. The gut as a sensory organ. *Nat. Rev. Gastroenterol. Hepatol.* **10**, 729–740 (2013).
6. Hu, D. & Reeves, P. R. The remarkable dual-level diversity of prokaryotic flagellins. *mSystems* **5**, e00705–e00719 (2020).
7. The Bohórquez Lab at Duke University. A gut sense for a microbial pattern regulates feeding. *YouTube* https://www.youtube.com/watch?v=3vXD_SXKT5U (2025).
8. von Uexküll, J. *Umwelt und Innenwelt der Tiere* (Springer, 1909).
9. Yong, E. *An Immense World: How Animal Senses Reveal the Hidden Realms around Us* (Random House, 2022).
10. de Hoyos-Vega, J. M. et al. Modeling gut neuro–epithelial connections in a novel microfluidic device. *Microsyst. Nanoeng.* **9**, 144 (2023).
11. Servin-Vences, M. R. et al. PIEZO2 in somatosensory neurons controls gastrointestinal transit. *Cell* **186**, 3386–3399 (2023).
12. Bayrer, J. R. et al. Gut enterochromaffin cells drive visceral pain and anxiety. *Nature* **616**, 137–142 (2023).
13. Bohórquez, D. V., Chandra, R., Samsa, L. A., Vigna, S. R. & Liddle, R. A. Characterization of basal pseudopod-like processes in ileal and colonic PYY cells. *J. Mol. Histol.* **42**, 3–13 (2011).
14. Bohórquez, D. V. et al. An enteroendocrine cell–enteric glia connection revealed by 3D electron microscopy. *PLoS ONE* **9**, e89881 (2014).
15. Lu, V. B. et al. Adenosine triphosphate is co-secreted with glucagon-like peptide-1 to modulate intestinal enterocytes and afferent neurons. *Nat. Commun.* **10**, 1029 (2019).
16. Hayashi, M. et al. Enteroendocrine cell lineages that differentially control feeding and gut motility. *Elife* **12**, e78512 (2023).
17. Bai, L. et al. Enteroendocrine cell types that drive food reward and aversion. *Elife* **11**, e74964 (2022).
18. Liu, W. W. & Bohórquez, D. V. The neural basis of sugar preference. *Nat. Rev. Neurosci.* **23**, 584–595 (2022).
19. Gribble, F. M. & Reimann, F. Enteroendocrine cells: chemosensors in the intestinal epithelium. *Annu. Rev. Physiol.* **78**, 277–299 (2016).
20. Martínez-Gury, K., Leone, V. & Chang, E. B. Regional diversity of the gastrointestinal microbiome. *Cell Host Microbe* **26**, 314–324 (2019).
21. Vijay-kumar, M. et al. Metabolic syndrome and altered gut microbiota in mice lacking Toll-like receptor 5. *Science* **344**, 228–232 (2010).
22. O'Donnell, M. P., Fox, B. W., Chao, P. H., Schroeder, F. C. & Sengupta, P. A neurotransmitter produced by gut bacteria modulates host sensory behaviour. *Nature* **583**, 415–420 (2020).
23. Ye, L. et al. Enteroendocrine cells sense bacterial tryptophan catabolites to activate enteric and vagal neuronal pathways. *Cell Host Microbe* **29**, 179–196 (2021).
24. Gabanyi, I. et al. Bacterial sensing via neuronal Nod2 regulates appetite and body temperature. *Science* **376**, eabj3986 (2022).
25. Tolhurst, G. et al. Short-chain fatty acids stimulate glucagon-like peptide-1 secretion via the G-protein-coupled receptor FFAR2. *Diabetes* **61**, 364–371 (2012).
26. Lin, V. H. et al. Butyrate and propionate protect against diet-induced obesity and regulate gut hormones via free fatty acid receptor 3-independent mechanisms. *PLoS ONE* **7**, e35240 (2012).

27. Chimere, C. et al. Bacterial metabolite indole modulates incretin secretion from intestinal enteroendocrine L cells. *Cell Rep.* **9**, 1202–1208 (2014).
28. Chassaing, B., Ley, R. E. & Gewirtz, A. T. Intestinal epithelial cell toll-like receptor 5 regulates the intestinal microbiota to prevent low-grade inflammation and metabolic syndrome in mice. *Gastroenterology* **147**, 1363–1377 (2014).
29. Chiu, I. M. et al. Bacteria activate sensory neurons that modulate pain and inflammation. *Nature* **501**, 52–57 (2013).
30. Sgritta, M. et al. Mechanisms underlying microbial-mediated changes in social behavior in mouse models of autism spectrum disorder. *Neuron* **101**, 246–259 (2018).
31. Muller, P. A. et al. Microbiota modulate sympathetic neurons via a gut–brain circuit. *Nature* **583**, 441–446 (2020).
32. Fülling, C., Dinan, T. G. & Cryan, J. F. Gut microbe to brain signaling: what happens in vagus.... *Neuron* **101**, 998–1002 (2019).
33. Margolis, K. G., Cryan, J. F. & Mayer, E. A. The microbiota-gut-brain axis: from motility to mood. *Gastroenterology* **160**, 1486–1501 (2021).
34. Bravo, J. A. et al. Ingestion of *Lactobacillus* strain regulates emotional behavior and central GABA receptor expression in a mouse via the vagus nerve. *Proc. Natl Acad. Sci. USA* **108**, 16050–16055 (2011).
35. Sagan, L. On the origin of mitosing cells. *J. Theoret. Biol.* **14**, 225–274 (1967).
36. Gewirtz, A. T., Navas, T. A., Lyons, S., Godowski, P. J. & Madara, J. L. Cutting edge: bacterial flagellin activates basolaterally expressed TLR5 to induce epithelial proinflammatory gene expression. *J. Immunol.* **167**, 1882–1885 (2001).
37. Hayashi, F. et al. The innate immune response to bacterial flagellin is mediated by Toll-like receptor 5. *Nature* **410**, 1099–1103 (2001).
38. Bogunovic, M. et al. Enteroendocrine cells express functional Toll-like receptors. *Am. J. Physiol. Gastrointest. Liver Physiol.* **7032**, 1770–1783 (2007).
39. Lundberg, J. M. et al. Localization of peptide YY (PYY) in gastrointestinal endocrine cells and effects on intestinal blood flow and motility. *Proc. Natl Acad. Sci. USA* **79**, 4471–4475 (1982).
40. Gehart, H. et al. Identification of enteroendocrine regulators by real-time single-cell differentiation mapping. *Cell* **176**, 1158–1173 (2019).
41. Billing, L. J. et al. Single cell transcriptomic profiling of large intestinal enteroendocrine cells in mice—identification of selective stimuli for insulin-like peptide-5 and glucagon-like peptide-1 co-expressing cells. *Mol. Metab.* **29**, 158–169 (2019).
42. Li, H. J. et al. Intestinal Neurod1 expression impairs paneth cell differentiation and promotes enteroendocrine lineage specification. *Sci. Rep.* **9**, 19489 (2019).
43. Rhee, S. H. et al. Pathophysiological role of Toll-like receptor 5 engagement by bacterial flagellin in colonic inflammation. *Proc. Natl Acad. Sci. USA* **102**, 13610–13615 (2005).
44. Sun, J., Fegan, P. E., Desai, A. S., Madara, J. L. & Hobert, M. E. Flagellin-induced tolerance of the Toll-like receptor 5 signaling pathway in polarized intestinal epithelial cells. *Am. J. Physiol. Gastrointest. Liver Physiol.* **292**, G767–G778 (2007).
45. Clasen, S. J. et al. Silent recognition of flagellins from human gut commensal bacteria by Toll-like receptor 5. *Sci. Immunol.* **8**, eabq7001 (2023).
46. Yao, Z. et al. A high-resolution transcriptomic and spatial atlas of cell types in the whole mouse brain. *Nature* **624**, 317–332 (2023).
47. Rakoff-Nahoum, S., Paglino, J., Eslami-Varzaneh, F., Edberg, S. & Medzhitov, R. Recognition of commensal microflora by toll-like receptors is required for intestinal homeostasis. *Cell* **118**, 229–241 (2004).
48. Thaiss, C. A. et al. Microbiota diurnal rhythmicity programs host transcriptome oscillations. *Cell* **167**, 1495–1510 (2016).
49. Dong, T. X. et al. T-cell calcium dynamics visualized in a ratiometric tdTomato-GCaMP6f transgenic reporter mouse. *Elife* **6**, e32417 (2017).
50. Batterham, R. L. et al. Gut hormone PYY3-36 physiologically inhibits food intake. *Nature* **418**, 650–654 (2002).
51. Abbott, C. R. et al. Blockade of the neuropeptide Y Y2 receptor with the specific antagonist BIIIE0246 attenuates the effect of endogenous and exogenous peptide YY (3–36) on food intake. *Brain Res.* **1043**, 139–144 (2005).
52. Koda, S. et al. The role of the vagal nerve in peripheral PYY3–36-induced feeding reduction in rats. *Endocrinology* **146**, 2369–2375 (2005).
53. Alonso, A. M. et al. The vagus nerve mediates the physiological but not pharmacological effects of PYY3-36 on food intake. *Mol. Metab.* **81**, 101895 (2024).
54. Kaelberer, M. M., Rupprecht, L. E., Liu, W. W., Weng, P. & Bohórquez, V. D. Neuropod cells: emerging biology of the gut-brain sensory transduction. *Annu. Rev. Neurosci.* **43**, 337–353 (2020).
55. Han, W. et al. A neural circuit for gut-induced reward. *Cell* **175**, 665–678 (2018).
56. Bai, L. et al. Genetic identification of vagal sensory neurons that control feeding. *Cell* **179**, 1129–1143 (2019).
57. McDougale, M. et al. Separate gut-brain circuits for fat and sugar reinforcement combine to promote overeating. *Cell Metab.* **36**, 393–407 (2024).
58. Williams, E. K. K. et al. Sensory neurons that detect stretch and nutrients in the digestive system. *Cell* **166**, 209–221 (2016).
59. Zhao, Q. et al. A multidimensional coding architecture of the vagal interoceptive system. *Nature* **603**, 878–884 (2022).
60. Luczynski, P. et al. Growing up in a bubble: using germ-free animals to assess the influence of the gut microbiota on brain and behavior. *Int. J. Neuropsychopharmacol.* **19**, pyw020 (2016).

Publisher's note Springer Nature remains neutral with regard to jurisdictional claims in published maps and institutional affiliations.

 **Open Access** This article is licensed under a Creative Commons Attribution-NonCommercial-NoDerivatives 4.0 International License, which permits any non-commercial use, sharing, distribution and reproduction in any medium or format, as long as you give appropriate credit to the original author(s) and the source, provide a link to the Creative Commons licence, and indicate if you modified the licensed material. You do not have permission under this licence to share adapted material derived from this article or parts of it. The images or other third party material in this article are included in the article's Creative Commons licence, unless indicated otherwise in a credit line to the material. If material is not included in the article's Creative Commons licence and your intended use is not permitted by statutory regulation or exceeds the permitted use, you will need to obtain permission directly from the copyright holder. To view a copy of this licence, visit <http://creativecommons.org/licenses/by-nc-nd/4.0/>.

© The Author(s) 2025

Methods

Mouse strains

All experiments on mice were performed following approval by the Institutional Animal Care and Use Committee at Duke University Medical Center under the protocol A212-21-10. Mice were group-housed in Duke University's Division of Laboratory Animal Resources, where they were kept on a 12-h light–dark cycle (0700–1900) with access to water and standard mouse chow (Purina 5001) ad libitum, unless otherwise indicated. The facility maintained an ambient temperature of 18–23 °C and humidity of 40–60%. Male and female adult mice aged 6–20 weeks were used in all experiments. The following experimental mouse strains were purchased, received or bred in-house and used directly: C57BL/6/J (JAX 000664), PYY–GFP¹³, CCK–GFP⁶¹, *Pyy*^{cre62}, NeuroD1–Cre (JAX 028364), loxP–STOP–loxP cassette (LSL)_tdTomato (JAX 007914), LSL_Halo–YFP (JAX 014539), LSL_ChR2–tdTomato (JAX 012567), LSL_Salsa6f (JAX 031968), *Tlr5*^{fl} (JAX 028599), *Myd88*^{fl} (JAX 008888), B6.Cg-*Snap23*^{tm3.1Hze}/J (JAX 025111) and *Fos*^{tm2.1(icre/ERT2)/Luo}/J (JAX 030323). The following double-transgenic mouse strains were bred in-house: *Pyy*^{cre};Salsa6f, NeuroD1–Cre_Salsa6f, *Pyy*^{cre};Halo–YFP and *Pyy*^{cre};ChR2–tdTomato. *Pyy*^{cre} mice were also bred to floxed *Tlr5*^{fl/fl} (floxed exon 4) and *Myd88*^{fl/fl} (floxed exon 3) mice to generate the following conditional knockout mice: *Pyy*^{cre}; *Tlr5*^{fl/fl} and *Pyy*^{cre}; *Myd88*^{fl/fl}.

Dissociation and isolation of single intestinal epithelial cells

Colons and small intestines of mice were dissociated for qPCR (PYY–GFP), calcium imaging (*Pyy*^{cre};Salsa6f) or sequencing (CCK–GFP and PYY–GFP) as previously described¹. In brief, the entire colon or proximal one-third of the small intestine was removed, flushed with cold PBS and cut into 2–3-mm sections. Tissue was rinsed with cold PBS and then shaken in 1.5 mM EDTA in PBS for 30 min before a 15-min incubation at 37 °C. The epithelial layer was then mechanically detached from the muscle layer by shaking in cold PBS. Following centrifugation at 800 r.p.m. (Eppendorf 5702 RH; rotor A-4-38), the pellet was resuspended and incubated in HBSS (Gibco) with dispase and collagenase for 10 min at 37 °C. Samples were then centrifuged (800 r.p.m.), filtered twice through a 70-μm and 40-μm filter, and resuspended in L15 medium (5% FBS, 10 μl ml⁻¹ 10 mM HEPES, 2,000 U ml⁻¹ penicillin–streptomycin and 100 μl of 1,700 U ml⁻¹ DNase) to produce a single-cell suspension for further analysis. For whole-epithelial-layer analyses, first the pellet was resuspended in lysis buffer and further processed for RNA extraction.

Dissociation and isolation of single nodose neurons

Nodose neurons of mice were dissociated for qPCR (C57BL/6J), calcium imaging (NeuroD1–Cre;Salsa6f) or sequencing (C57BL/6J) as previously described¹. In brief, nodose ganglia were dissected and immediately placed into 500 μl of ganglia dissociation solution containing 10 mM HEPES, 1× glutamine, 1× N2 supplement, 1× B27 supplement, 0.5 μg ml⁻¹ nerve growth factor and 55 μg ml⁻¹ liberase (Roche, 5401054001) in Advanced DMEM/F-12. Following digestion, ganglia were rinsed twice with PBS, mechanically dissociated in dissociation solution, and filtered through a 70-μm cell strainer. The dissociated solution was then carefully laid on a density gradient of 500 μl 12% and 500 μl 28% Percoll (Sigma) and centrifuged for 10 min at 2,900g at room temperature. Once centrifugation was complete, the top 700 μl was removed, and 700 μl of fresh dissociation solution was added. Cells were then centrifuged for 15 min at 2,900g, and the final pellet was resuspended in 500 μl PBS plus 0.04% BSA.

RNA sequencing

RNA was extracted from single-cell suspensions using the Single Cell RNA Purification Kit (Norgen). All samples were assessed with a Bioanalyzer (Agilent), and only samples with RNA integrity number scores >8.0 were used for downstream analysis. Given the rarity of

the cells, Single-cell RNA barcoding sequencing was used to generate libraries. Libraries were sequenced on an Illumina NextSeq 500. STAR was used with the mm10 mouse reference genome to align reads, and count tables were generated using featureCounts. Pairwise comparisons between genes from the PYY–GFP⁺ and PYY–GFP⁻ groups were made using DESeq2. Gene ontology analyses were conducted using topGO.

qPCR

The colonic epithelium of PYY–GFP mice was dissociated, and cells were sorted as described above. An equal number of GFP⁺ and GFP⁻ cells were collected directly into lysis buffer. Whole epithelium was dissociated from *Pyy*^{cre}; *Tlr5*^{fl/fl} and *Tlr5*^{fl/fl} control littermates and collected into lysis buffer as described above. Nodose was dissected and flash-frozen in liquid nitrogen. RNA was extracted on the basis of the manufacturer's protocol using the RNeasy Micro Plus Kit (Qiagen no. 74034). Spleen and whole-colon tissues were collected and homogenized in TRIzol reagent (Thermo Fisher, 15596026), and RNA was extracted per the manufacturer's protocol. cDNA was produced per the manufacturer's protocol using the High-Capacity cDNA Reverse Transcription Kit (Applied Biosystems, 4368814). The following TaqMan probes were used for transcript identification: *Pyy* (Mm00520716_g1), *18s* (Mm03928990_g1), *Tlr1* (Mm00446095_m1, Mm01208874_m1), *Tlr2* (Mm00442346_m1, Mm01213946_g1), *Tlr3* (Mm01207404_m1), *Tlr4* (Mm00445273_m1), *Tlr5* (Mm00546288_s1), *Actb* (Mm02619580_g1), *Tnf* (Mm00443258_m1), *Il1b* (Mm00434228_m1), *Il6* (Mm00446190_m1), *Tjp1* (Mm01320638), *Tjp2* (Mm00495620_m1), *Ocln* (Mm00500910_m1) and *Cldn* (Mm01342184). qPCR was run on a StepOnePlus System (Thermo Fischer), using TaqMan Fast Universal PCR Master Mix (Applied Biosystems no. 4352042) according to the manufacturer's protocol. Transcription rate was determined as 2^{-ΔCt} or compared as fold change using 2^{-ΔΔCt}. All values are reported as mean ± s.e.m.

In situ hybridization with immunofluorescence

NeuroD1_tdTomato and PYY–GFP mice were transcardially perfused with PBS for 3 min followed by 4% PFA for 3 min at a rate of 600 μl min⁻¹. The entire intestine was collected, opened lengthwise and divided into different sections: proximal, middle and distal third of the small intestine; and proximal and distal halves of the large intestine. Intestinal tissue was then rolled with the proximal end in the centre, and post-fixed in 4% PFA for 24 h. Nodose ganglia and dorsal root ganglia at the levels of L5, L6 and S1 were also dissected bilaterally. Neuronal ganglia were rinsed in PBS and post-fixed in 4% PFA for 24 h. Tissue was then dehydrated in 10% sucrose for 1 h and 30% sucrose for at least 12 h. Samples were embedded in OCT (VWR) and stored at –80 °C. Tissue was sectioned onto slides at 16 μm using a cryostat. RNA detection was performed using the RNAscope Multiplex Fluorescent Reagent Kit v2 Assay (ACD). In brief, tissue slides were baked for 30 min at 60 °C, and post-fixed in 10% neutral buffered formalin (VWR) for 60 min before being washed in PBS twice (Sigma). Slides were then dehydrated using successive alcohol washes of 50%, 70% and 100%, and a second 100% of ethanol for 5 min each. Slides were then incubated with hydrogen peroxide for 10 min before undergoing target retrieval using RNAscope reagents in a steamer. Slides were submerged into the RNAscope target retrieval solution at >99 °C for 5 min. Slides were then treated with protease III for 30 min at 40 °C before subsequent hybridization and amplification steps per the manufacturer's instructions. The probes used were all purchased from ACD: Mm-Tlr5 (catalogue no. 468888), Mm-Pyy-C3 (catalogue no. 420681) and Mm-Npy2r (catalogue no. 515431). Hybridization signal was detected using Opal dyes (Akoya Biosciences) at a dilution of 1:1,500. Tissue was then blocked in 10% donkey serum (Jackson ImmunoResearch) for 1 h. Tissue was then incubated with primary antibody dissolved in antibody dilution solution (PBS with 1% BSA and 0.0025% Triton X-100) for 24 h at 4 °C, followed by 1 h at room temperature. Primary antibodies and dilutions were as follows: Rb-anti-PYY (1:250; gift from the Liddle

Article

laboratory), Rb-anti-PGP9.5 (1:500; Abcam: ab27053), Gt-anti-serotonin (1:500; Abcam, ab66047) and CHK-anti-GFP (1:500; Abcam: ab13970). Following primary antibody incubation, tissue was washed in 0.05% Tween-20 in TBS buffer (TBST) and then incubated with secondary antibody in antibody dilution solution for 1 h at room temperature: Dk-anti-Rb-488 (1:250, catalogue no. 711-546-152), Dk-anti-Rb-Cy3 (1:250, catalogue no. 11-166-152), Dk-anti-Ck-488 (1:250, catalogue no. 703-546-155), Dk-anti-Gt-647 (1:500, catalogue no. 705-606-147), all from Jackson ImmunoResearch. Tissue was then washed with TBST, stained with DAPI (1:4,000) for 10 min, washed in TBST, and mounted using Fluoro-Gel with Tris buffer (Electron Microscopy Sciences). Imaging was carried out on a Zeiss 880 Airyscan inverted confocal microscope. Images were adjusted for brightness and contrast using ImageJ (Fiji V.2.9.0). In each region of the intestine, the 50 most proximal cells were analysed from a total of $n = 3$ mice. Cells with >2 puncta within the cell body were considered positive for the gene. Control slides using the negative control probes (ACD) were used to ensure that background staining was <3 puncta per cell. Counts are presented as the mean percentage of co-localization \pm s.e.m.

Assessment of basal phenotypes

Pyy^{cre};Tlr5^{fl/fl}, *Pyy^{cre};Myd88^{fl/fl}* and their Cre-negative littermates were weighed following weaning, and every week thereafter until 3 months of age. Mice were then euthanized, and colon length, colon weight and spleen weight were measured. Colonic tissues were flushed with cold PBS, incubated in 10% neutral buffered formalin (VWR) for ≥ 24 h at 4 °C, dehydrated in a graded series of ethanol and embedded in paraffin. Tissues were sectioned and stained with haematoxylin and eosin (Abcam, ab245880) per the manufacturer's protocol and imaged for assessment of developmental and immune phenotypes.

Measurement of food intake

Age-matched *Pyy^{cre};Tlr5^{fl/fl}* and littermates were placed into clean cages with food hoppers. The hoppers are designed to minimize the ability of mice to remove entire pellets. The weight of the food in the hopper was recorded at both the start and end of a 24-h period. Mice were then returned to their home cage for at least 2 days before repeating the test twice more. The mean of three separate testing days for each individual mouse is reported.

Detailed feeding, activity and meal pattern analysis

Age- and sex-matched *Pyy^{cre};Tlr5^{fl/fl}*, *Pyy^{cre};Myd88^{fl/fl}* and their Cre-negative littermates were placed in a custom-built PhenoMaster behavioural phenotyping system for 10 days (TSE Systems). The first week was considered an acclimation period, and all meal pattern analyses were performed on the last 3 days within the system. The PhenoMaster was programmed (software version 6.6.9) to automatically maintain a light cycle (07:00 lights on; 19:00 lights off), temperature control (22 °C) and humidity control (40%). The PhenoMaster holds 12 clear cages, in which animals were singly housed. Cages were industrially washed, and bedding (ALPHA-dri) was replaced weekly. Animals were provided with standard mouse chow (Purina 5001) and reverse-osmosis water ad libitum. All cages also housed an enrichment device, which also served to weigh the animals. Food hopper, water bottle and weigh container were attached to weight sensors (TSE). Food intake, water intake and weight were automatically measured every 5 s to the nearest 0.01 g. For drinking measurements, a 10-s smoothing interval with a maximum raw analog-to-digital conversion count difference of 40,000 was permitted. For weight measurements, a 15-s smoothing interval with a 15-g threshold and a maximum raw analog-to-digital conversion count difference of 1,000,000 was permitted. Intake was measured every 5 s and binned every minute for analyses unless otherwise indicated. Animal activity was determined by beams crossed in the x and y planes and was collected with a 100-Hz scan rate. Unless otherwise indicated, all activity, food intake and water intake measurements were

binned in 1-min intervals for analysis. Data were corrected for minor fluctuations by only permitting a monotonically increasing function for both food and water intake: values that represented negative food intake were replaced by the most recent value. Meal size, frequency and timing were defined on the basis of parameters within the PhenoMaster system. Inter-meal intervals were required to be >10 min. Only meals of size 0.1–1 g and rate <0.25 g min⁻¹ were included in the meal pattern analysis.

Fasting blood glucose and oral glucose tolerance test

Blood glucose was measured in age-matched *Pyy^{cre};Tlr5^{fl/fl}* and *Tlr5^{fl/fl}* mice following an overnight fast of 18 h. For oral glucose tolerance test, a separate cohort of mice were food- and water-deprived for 5 h. Then, mice were gavaged with sucrose (2 g kg⁻¹ body weight in sterile PBS). Blood glucose was measured (True Metrix 60 Blood Glucose Meter) after the deprivation, and 15, 30, 60, 90 and 120 min following gavage.

Fecal lipocalin-2 measurements

Colonic inflammation was assessed by assaying for fecal lipocalin-2 using an ELISA (Ray Biotech). Stool samples were collected from age-matched *Pyy^{cre};Tlr5^{fl/fl}* and Cre-negative controls during the beginning of the light cycle. Fecal samples were reconstituted in PBS to a final concentration of 100 mg ml⁻¹ and vortexed for 5 min to obtain a homogeneous mixture. Fecal matter was then centrifuged for 10 min at 14,000g. Supernatants were collected and stored at -80 °C. Lipocalin-2 levels were assessed following the manufacturer's instructions, and optical density was measured at 450 nm (Tecan Infinite 200 Pro).

Colonic myeloperoxidase assay

Neutrophil activity in tissue was assessed by testing for the enzymatic activity of myeloperoxidase using a colorimetric kit (Abcam). A 2–3-mm segment of the distal colon from age- and sex-matched *Pyy^{cre};Tlr5^{fl/fl}* and littermates was dissected and weighed. Tissue was then washed in PBS, and mechanically homogenized in the lysis buffer provided in the kit. Tissue was then freeze-thawed twice and sonicated. Myeloperoxidase activity was assessed following the manufacturer's protocol and normalized to the tissue mass, and optical density was measured at 450 nm (Tecan Infinite 200 Pro).

Serum hormone measurement

Age-matched *Pyy^{cre};Tlr5^{fl/fl}* and Cre-negative controls were fasted for 15 h and then fed ad libitum for 2 h. Following the re-feeding period, mice were euthanized, and serum was collected. DPP-4 inhibitor and aprotinin were added to serum samples to prevent peptide degradation. Total PYY3-36 (RayBiotech) and total GLP-1 (Alpco) levels were assessed using an ELISA per the manufacturer's protocols.

Stool flagellin assay

Flagellin levels were assessed using HEK-Blue-mTLR5 cells (Invivo-gen). Stool was collected from age-matched wild-type, *Pyy^{cre};Tlr5^{fl/fl}* and Cre-negative controls during the start of the light cycle, following ad libitum feeding, an 18-h overnight fast or an 18-h overnight fast followed by a flagellin enema (1 µg ml⁻¹ in 100 µl). Fecal material was resuspended in PBS to a final concentration of 100 mg ml⁻¹. Solutions were mechanically homogenized and vortexed for 5 min to form a suspension. Samples were then centrifuged at 8,000g for 2 min, and serum was collected and either immediately assessed or stored at -20 °C for later testing. Serial dilutions of the solution were placed onto the HEK-TLR5 cells, and purified *S. typhimurium* flagellin (Invivo-gen) was used to generate a standard curve. After 18 h of stimulation, cell culture supernatant was applied to QUANTI-Blue medium and incubated for 30 min at 37 °C. QUANTI-Blue alkaline phosphatase activity was then read at 620 nm (Tecan Infinite 200 Pro).

Calcium imaging of dissociated cells

For neurons, NeuroD1-Cre_Salsa6f nodose neurons were dissociated as described above. Neurons were plated on 12-mm coverslips and placed in a 37 °C incubator overnight. Neuronal medium included: 1× GlutaMAX, 10 mM HEPES, 200 U ml⁻¹ penicillin–streptomycin, 1× N2 supplement, 1× B27 supplement and 10 ng ml⁻¹ nerve growth factor in Advanced DMEM/F-12. Cells were imaged 2–3 days after plating. For enteroendocrine cells, NeuroD1Cre_Salsa6f cells were dissociated as described above and fluorescence-sorted (BD FACSARIA), selecting for tdTomato⁺ fluorescent cells. Cells were then plated on coverslips coated with 2.5% Matrigel (Corning no. 356231). Enteroendocrine cells were imaged 2–6 h after plating. Cells were washed twice in imaging buffer (120 mM NaCl, 3 mM KCl, 2 mM CaCl₂, 2 mM MgCl₂, 10 mM HEPES, 10 mM glucose; 305 mOsm ± 3 mOsm) and placed in the dark for 5 min until they reached room temperature. Coverslips were then placed in the recording chamber of a Zeiss Examiner Z1 and imaged with a Hamamatsu camera (Orca-flash4.0; C11440) using the Zeiss ZEN Blue software package. GCaMP6f emission images were obtained using 570-nm excitation. Images were collected at 1.5-s intervals with a 100-ms exposure time. Each recording was 180 s long, with a stimulus perfused between 30 and 60 s. Imaging buffer was continuously perfused (about 2 ml min⁻¹) over the coverslips throughout the imaging session. Each coverslip underwent four recordings: buffer, test stimulus, repeat of the test stimulus, and KCl. Each recording session concluded with 50 mM KCl as an activity control (KCl concentration was achieved by substituting for NaCl, and not an addition of more KCl). A response to KCl was defined as a ratio >10% increase above baseline. Cells that did not reach this KCl threshold were not included in analyses. A 5-min wash-out period with continuous perfusion of imaging buffer was carried out between the two test stimuli. For experiments involving the TLR5 inhibitor, TH1020 was added to the well to reach a final concentration of 1 µM following the wash-out period. Buffer flow was stopped, and cells were incubated with the inhibitor for 10 min before restarting flow and retesting with the stimulus.

Analysis. Fluorescence values for each individual cell were calculated as the mean fluorescence intensity in a user-defined region of interest on Fiji software. Intracellular calcium changes were then calculated as $\Delta F/F = (F - F_0)/F_0$, in which F_0 is the average intensity of the cell within the first 15 s. Ratiometric values were then normalized to the peak KCl response. A positive response was defined as an increase in ratio >10% above baseline.

PYY release assay

Colons from wild-type and knockout mice were dissected, flushed with cold PBS, opened lengthwise and cut into pieces of about 1 cm. Tissue pieces were incubated on ice in PBS for 2 h before incubation with 1.5 mM EDTA on ice for 30 min, and then 37 °C for 15 min. Crypts were detached by shaking in cold PBS, pelleted at 100g and plated on 12-mm coverslips coated with 2.5% Matrigel (Corning no. 356231). Crypts were then incubated in 50% L-WRN Buffer (ATCC) with 10 µM Y-27632 (Enzo) for 16 h before stimulation. Crypts were then stimulated with buffer (120 mM NaCl, 3 mM KCl, 2 mM CaCl₂, 2 mM MgCl₂, 10 mM HEPES, 10 mM glucose), 100 ng ml⁻¹ flagellin in buffer, or a mixture of 1 µM IBMX (Sigma) and 1 nM forskolin (Sigma) in buffer for 30 min at 37 °C. Supernatant was collected, and the crypts were then incubated in lysis buffer for 30 min at 4 °C. Lysate was collected, and both lysate and supernatant were centrifuged for 10 min at 13,000g to remove insoluble material, and stored at -20 °C for up to 2 weeks. PYY concentration in samples was assessed using the PYY ELISA Kit (Ray BioTech) following the manufacturer's protocol. Each experimental condition was run in duplicate on every plate. A PYY standard was run for every plate. Absorbance at 450 nm was measured on a plate reader (Tecan Infinite 200 Pro). PYY amount and concentration was calculated

using the standard curve. PYY release was calculated as supernatant/(supernatant + lysate).

Vagus nerve recordings

Whole-nerve recordings were performed in wild-type mice, *Pyy*^{cre}; Halo-YFP mice, *Pyy*^{cre}; Chr2 mice, *Pyy*^{cre}; *Tlr5*^{fl/fl} mice, *Pyy*^{cre}; *Myd88*^{fl/fl} mice and negative genetic controls. Whole-nerve electrophysiology recordings of the cervical vagus nerve were performed as previously reported⁴. A 20-gauge gavage needle with two connected tubes for PBS perfusion and stimulant delivery was surgically inserted through the caecum wall into the proximal colon. A perfusion exit incision was made just proximal to the rectum for colon. Fecal pellets were gently expressed from the colon using cotton applicators. PBS was constantly perfused through the isolated intestinal region at about 400 µl min⁻¹ as a baseline and volume pressure control. Stimulation conditions were applied after recording 2 min of baseline activity. During stimulation conditions, PBS perfusion was continuous, and 200 µl of 2 µg ml⁻¹ flagellin was perfused over 1 min using a syringe pump (Fusion 200, Chemyx). As a positive control to activate the vagus nerve from the colon lumen, intralipid (7%, Sigma) was infused.

Data acquisition. Extracellular voltage was recorded as previously described⁴. The raw data were analysed using Spike Tailor, a custom MATLAB software (Mathworks) script⁴. Spikes were detected using a threshold detected on the basis of root-mean-square noise. The firing rate was calculated using a Gaussian kernel smoothing algorithm in 200-ms bins.

Optogenetic inhibition and stimulation. The optoelectronic colon fibre was threaded along the gavage needle into the colonic lumen. MicroLED stimulation was applied simultaneously with nutrient infusion. The microLED was pulsed for 1 min at 40 Hz, 5 V peak and 20% duty cycle (473 nm, 532 nm).

Pharmacologic inhibition. Following recording of a pre-inhibitor response, the inhibitor was delivered over 1 min (10 µl g⁻¹ BIIE-0246) and allowed to incubate for 10 min before re-infusion of flagellin.

Data analysis. Stimulation response was quantified as the maximum firing rate after stimulation (stimulant conditions) or during recording (baseline). Each trial served as its own control by normalizing the firing rate to the pre-stimulus baseline firing rate (first 2 min of recording). Throughout experiments, intralipid response was used as a positive control. For all nutrient and laser stimulation conditions, data were excluded if an intralipid response was not seen throughout the recording session. Maximum firing rate and area under the curve were analysed across stimulation condition.

Optoelectronic colon fibre fabrication

The preform assembly for optoelectronic graded-index fibres began with moulding polystyrene-block-poly(ethene-co-butadiene)-block-polystyrene (SEBS) pellets (Kraton G1657M) into desired geometrical patterns in a CNC machined inverse aluminium mould at 200 °C for 8 h under vacuum. The top layer defined the hollow square channels (3.6 mm × 3.6 mm × 30 cm) with a pitch size of 4 mm for hosting the interconnect microwires. The SEBS convergence channels were subsequently lined with a U-shaped PC layer that had a wall thickness of 1 mm and channel size of 1.6 mm × 1.6 mm produced by standard CNC machining process. This preform was consolidated in an oven (130 °C, 45 min) and subsequently drawn into metres-long microscale fibres at a size reduction ratio of 40–45, while simultaneously feeding three spools of 40-µm Ag–Cu microwires.

Fibre device fabrication. Fabrication of graded-index fibre device began with dissolving away the SEBS layer in the distal 1 cm of fibre

Article

(8.5 cm total length) in dichloromethane for 10 min, which exposed the interconnect microwires. The interconnects were subsequently soldered onto male header pins that were assembled inside a custom 3D-printed box (5 mm × 7 mm × 0.5 mm) and secured using UV curable epoxy. About 0.5 cm of the interconnect microwires was exposed by low-end machining with a razor blade at the distal end of the fibre under an optical microscope, followed by mounting of blue (473-nm emission maxima) and green (532-nm emission maxima) In_xGa_{1-x}N microLED chips (CREE TR2227 and SR2130) using two-part silver epoxy (Epo-tek). Subsequently, a 10-μm layer of vapour-deposited parylene-C defined the bio-fluid barrier layer. Finally, the device was encapsulated in an approximately 50–100-μm layer of medical-grade silicone by inserting the fibre device in a PTFE tubing with an inner diameter of 0.8 mm, which acted as a sacrificial mould. The silicone mixture was filled and cured in the tubing, and subsequently the tubing was cut open to yield a silicone-coated soft device. The final fibre had an overall length of 8.5 cm with three green and blue microLEDs hosted on the distal 2 cm of the fibre at a separation of 1 cm.

In vivo two-photon calcium imaging and compartment analysis of temporal activity by fluorescence in situ hybridization

Snap25-FosTRAP-tdTomato triple-transgenic mice were used to generate landmark tdTomato⁺ vagal nodose neurons for compartment analysis of temporal activity by fluorescence in situ hybridization (catFISH) analysis through targeted recombination in active populations (TRAP) at least 10 days before calcium imaging as previously described⁵⁷. In brief, 6-h-fasted mice were given intragastric infusions of nutrients (500 μl; 100 μl min⁻¹) 30 min before dark cycle onset. At 3 h after stimulus delivery, mice were injected with 4-hydroxytamoxifen (30 mg kg⁻¹, intraperitoneal; Sigma) to induce tdTomato expression in a subpopulation of nutrient-responsive vagal sensory neurons, allowing for post hoc landmarking and alignment. Chow was returned 3 h after 4-hydroxytamoxifen injection. For calcium imaging, mice were fasted overnight (18 h) and maintained under continuous anaesthesia (isoflurane–oxygen) on a heating pad to sustain body temperature throughout the procedure. An abdominal incision was first made in the anaesthetized mice to expose the caecum and colon. A 20-gauge gavage needle with dual tubing for PBS perfusion and stimulant delivery was surgically inserted through the caecal wall into the proximal colon and secured with a suture. The rectum was severed to create an exit for fluid drainage. Fecal pellets were gently expelled from the colon using cotton applicators. Next, an incision (about 2 cm) was made above the sternum and below the jaw. The carotid artery and vagus nerve were exposed by separating the salivary glands. Retractors were used to pull the sternomastoid, omohyoid and posterior belly of the digastric muscle aside to visualize the nodose ganglion. The vagus nerve was transected just above the nodose ganglion, which was carefully separated from the hypoglossal nerve and small adjacent branches. The vagus nerve was then dissected away from the carotid artery and surrounding tissues. The right nodose ganglion was gently positioned on a stable imaging platform consisting of a 5-mm-diameter coverslip attached to a metal arm fixed to a magnetic base. Surgical silicone adhesive (Kwik-Sil, WPI) was applied to immobilize the vagus nerve on the coverslip, and the nodose ganglion, immersed in Dulbecco's modified Eagle medium (Corning), was covered with a second coverslip before imaging.

Stimulus perfusion. Perfusions were performed using a precision pump connected to silicone tubing filled with PBS, flagellin (2 μg ml⁻¹) or 7% intralipid. PBS (1,000 μl min⁻¹) was continuously perfused throughout the recording. Baseline neuronal activity was recorded for 30 s, followed by a 2-min flagellin infusion (333 μl min⁻¹) and an additional 2 min of recording post-infusion.

In mice in which responses to both flagellin and intralipid were tested, the colon was flushed with 10 ml of PBS after flagellin perfusion to remove residual flagellin through the exit port. A second baseline

activity recording was then taken, followed by a 2-min intralipid perfusion (333 μl min⁻¹) and another 2-min post-perfusion recording.

Imaging. In vivo imaging was performed using a two-photon microscope (Bruker) equipped with a galvanometer for image acquisition and a piezo objective combined with a galvo/resonant scanner, enabling image capture at 29 frames per second (Prairie View v.5.7). The microscope was set up for in vivo conditions with a Somnosuite (isoflurane) anaesthesia device coupled to a homeothermic control warming pad (Kent Scientific) and a programmable syringe pump (Harvard Apparatus PHD 2000) for nutrient perfusion into the gut. Imaging was conducted using a 16× water-immersion upright objective.

RNAscope and alignment. For nodose catFISH analysis, we adapted a previously reported protocol for registration of vagal neurons between in vivo calcium imaging and RNAscope fluorescent in situ hybridization images⁵⁹. After in vivo imaging, immobilized nodose ganglia were immediately fixed in 4% PFA for 2 h and then placed in 30% sucrose for 1 h before being embedded in OCT and frozen at -20 °C. Nodose ganglia were then sliced into 10-μm sections, and an RNAscope assay was performed to probe for *Npy2r* mRNA expression as described above, without slide baking, post-fixation and target retrieval. To align RNAscope sections to in vivo imaging z-stacks, 'guidepost' neurons were used as positional landmarks for mapping between in vivo and sectioned images. In brief, tdTomato⁺ neurons visible in both RNAscope sections and in vivo planes were identified as landmark reference points and were manually paired using the BigWarp tool within the Fiji BigDataViewer plugin. Using this tool, RNAscope sections were transformed and aligned to corresponding planes within the in vivo imaging z-stack, allowing visualization of NPY2R⁺ neurons overlaid on GCaMP6s-fluorescent neurons. Cells with ambiguous or unsuccessful alignment were not used for further analysis.

Quantification of neural activity. GCaMP6s fluorescence changes were quantified by outlining regions of interest (ROIs), each corresponding to a single cell throughout the imaging session. For nodose images processed using catFISH alignment, ROIs were selectively generated around NPY2R⁺ cells. Pixel intensities in ROIs (average across pixels) were calculated frame by frame using ImageJ and exported to Excel for analysis. The z-score for each neuron was calculated by subtracting the mean baseline fluorescence (over a 30-s period) from the fluorescence intensity at each time point and dividing by the standard deviation of the baseline fluorescence. This normalized value represents the number of standard deviations from the baseline fluorescence. A neuron was considered responsive if: the peak GCaMP6s fluorescence reached a z-score of ≥2.5, and the mean GCaMP6s fluorescence was ≥2.5 above the baseline mean for at least 5 s during or after infusion. Neurons without baseline activity were excluded from the analysis.

Food intake behavioural system

Mice were acclimated to enema two times before the start of the test. Tests were started 3 h into the start of the light cycle. Mice were fasted overnight for 18 h. At the start of the test, mice received a 100-μl enema of 1 μg ml⁻¹ flagellin or PBS and were then placed into a clean cage. A pre-weighed pellet of standard rodent chow (5001 Purina) was then introduced to the cage, and then weighed at 20, 40, 60 and 180 min following the enema. At the end of the test, mice were returned to their home cages. The start of all test sessions was separated by at least 48 h. For pharmacological inhibition of TLR5, C57BL/6J wild-type mice were acclimated to enema, a baseline response to flagellin was established, and then mice received enemas of 1 μg ml⁻¹ flagellin or PBS combined with 10 μM TH1020 (Sigma). Food intake was then measured as described above.

For pharmacologic inhibition of Y2 receptors with intraperitoneal injections, C57BL/6J wild-type mice were acclimated to enema and

intraperitoneal injections two times before the start of the test. At the start of the test, mice received an intraperitoneal injection with 2 ng kg⁻¹ BIIE-0246 or vehicle and were then placed into a clean cage. After 10 min, mice received a 100-μl enema of 1 μg ml⁻¹ flagellin or PBS. Food intake was then measured as described above.

Germ-free mice. Age- and sex-matched germ-free C57BL/6J wild-type mice were transferred from the Duke Gnotobiotic core in sterile, individual cages. Tests were started 3 h into the start of the light cycle. Mice were fasted overnight for 18 h. At the start of the test, mice received a 100-μl enema of PBS, followed by an enema 1 μg ml⁻¹ flagellin 7 days later. Food intake was measured as described above.

Crunch Master behavioural system

Female and male, 8-week-old, wild-type C57BL/6J mice were habituated for 1 h a day for 2 days in the behavioural device before the test session. Mice were food-deprived 18 h before the test session, which was performed during the light phase of the mice. Preceding the test session, mice were weighed and subsequently administered a 100-μl enema of either 1 μg ml⁻¹ flagellin or PBS. Immediately following the enema administration, the mice were placed into the acrylic box and allowed to feed ad libitum for 1 h. After the test session, the mice were returned to their home cages.

Behavioural device. An acrylic box (37 cm × 27 cm) was equipped with a microphone (FIFINE T-669) attached to one wall. To enhance sound recording, 12 small drill holes (0.5 cm diameter) were incorporated into the wall near the microphone. A video camera (Kayeton Technology, model KYT-U400-MCS2812R01) was positioned 57 cm beneath the acrylic box to capture a bottom-up view of the mouse's feeding behaviour. On the same wall as the microphone, a single standard chow food pellet was glued to a plastic lid that was then affixed to the wall. The weight of the food pellet was measured both before and after the test session to calculate food intake, with adjustments made for any food spillage. The audio and video data were recorded using the OBS 29.1.3 software.

Audio processing. Audio recordings were converted into .ogg format. Initial recordings were captured at a sampling frequency of 44.1 kHz, and then subsampled to 2,205 Hz for power spectrogram computation. The biting frequency was determined to lie between 400 and 1,000 Hz, the absolute power spectrum was averaged, and a band-pass filter between 400 and 1,000 Hz was applied to accurately identify biting frames. From the filtered signal, a threshold of 0.5 standard deviations above the mean was calculated. Each audio frame exceeding this threshold was binarized to 1 (indicating a potential bite), whereas those below were set to 0 (non-bite). This procedure further helped to eliminate false bite events. The binarized signal was then used to compute the bite start and end. A bite was defined as a sequence of binarized audio frames (with values of 1) separated by pauses in feeding (values of 0) longer than 10 s. These pauses were referred to as inter-bite intervals. A minimum of three consecutive audio frames with a value of 1 was required to be considered a bite.

Video processing. To ensure accurate bite identification, video snippets were automatically generated for each potential bite event. These snippets were then reviewed and validated by a human observer. Only the video snippets depicting correctly identified bites were included in the subsequent analysis. All video snippets utilized in this study are available in the Supplementary Information. The original video footage was recorded in .mkv format at a frame rate of 30 frames per second.

Statistics and reproducibility

We performed statistical analyses using R (3.1) and JMP Pro (SAS, version 16), unless otherwise indicated. Data were evaluated for normality

using a *Q-Q* plot. For normally distributed data, ANOVA was used and Tukey HSD post hoc testing was performed when applicable. For behaviour studies, we used a repeated-measures ANOVA to account for each individual, followed by post hoc paired Student's *t*-tests. For data not normally distributed, means were evaluated by Kruskal–Wallis test with non-parametric comparisons using the Wilcoxon method. For other studies, comments on statistical tests performed are included throughout the Methods and in the figure legends. All error bars and shaded regions represent s.e.m. unless otherwise indicated. Sample size was not predetermined using power analyses. Standardized randomization was not performed for in vitro or in vivo experiments. All behavioural studies were counterbalanced across age and sex to control for variables including position in cage and order effect. Experimenters were not blinded to treatment condition, genotype or outcome.

Reporting summary

Further information on research design is available in the Nature Portfolio Reporting Summary linked to this article.

Data availability

All data supporting the findings of this study are available within the paper and its Supplementary Information. The mm10 mouse reference genome is available from GENCODE vM23/Ensembl 98. RNA-sequencing datasets are available on the NIH Gene Expression Omnibus (GEO) database under accession GSE288590. Data from single-cell RNA-sequencing analysis of whole mouse brain are available at ref. 46 or via the Allen Institute Brain Atlas at <https://portal.brain-map.org/atlas-and-data/bkp/abc-atlas>.

Code availability

The analysis code used for Crunch Master feeding behaviour analysis is available via the OSF at <https://doi.org/10.17605/OSF.IO/7XGFD>.

- Wang, Y. et al. Amino acids stimulate cholecystokinin release through the Ca²⁺-sensing receptor. *Am. J. Physiol. Gastrointest. Liver Physiol.* **300**, G528–G537 (2011).
- Schonhoff, S. et al. Energy homeostasis and gastrointestinal endocrine differentiation do not require the anorectic hormone peptide YY. *Mol. Cell. Biol.* **25**, 4189–4199 (2005).

Acknowledgements We thank J. Kotula and M. Toh for assistance with sequencing; R. A. Liddle, S. G. Lisberger, M. D. Gunn, J. A. Alspaugh, N. K. Surana, G. J. Schwartz, Z. Lorsch, M. Toc Sagra and E. B. Bohórquez for editorial input. We acknowledge the following funding sources: National Institutes of Health (NIH) F30 DK122712 (W.W.L.); NIH F32 DK139628 (N.R.); NIH F30 DK136229 (E.A.); NIH F32 DK127757 and NIH K01 DK138286 (L.E.R.); NIH F30DK127650 (P.W.); J.A.A.G. is a doctoral student from the Programa de Doctorado en Ciencias Biomédicas of the Universidad Nacional Autónoma de México and has received CONAHcyT fellowship no. CVU959984; CONAHcyT CF-2023-G-518 (R.G.); NIH K01 DK131403 (M.M.K.); and NIH DP2 MH122402, NIH R21 AT010818, NIH R03 DK114500, NIH R01 DK131112 and NIH R01 DK132070 (D.V.B.).

Author contributions W.W.L., N.R., E.A., L.E.R., P.W., C.S., M.E.K., J.A.V., C.P.-H., Y.G.K.A., A. Carbajal, J.A.A.G. and A. Coss conducted experiments and acquired data; A.S. and P.A. generated luminal optogenetic resources and optoelectronic microLED; E.G.-L. and R.G. developed the Crunch Master assay, conducted experiments, and acquired and analysed data; A.d.A., A.B. and G.d.L. conducted in vivo calcium imaging and catFISH, acquired and analysed data; W.W.L., N.R., E.A., L.E.R., P.W., J.F.R., E.A.M., M.M.K. and D.V.B. analysed and interpreted data. W.W.L., N.R., E.A., M.M.K. and D.V.B. conceptualized and wrote the manuscript with input from all authors. M.M.K. and D.V.B. developed the idea and supervised the project. D.V.B. acquired funding for the project.

Competing interests D.V.B. and M.M.K. are founders and board directors of the Gastronauts Foundation, Inc, a 501(c)3 non-profit company. Some of the findings have been filed by D.V.B. as a provisional patent application. All other authors declare no competing interests.

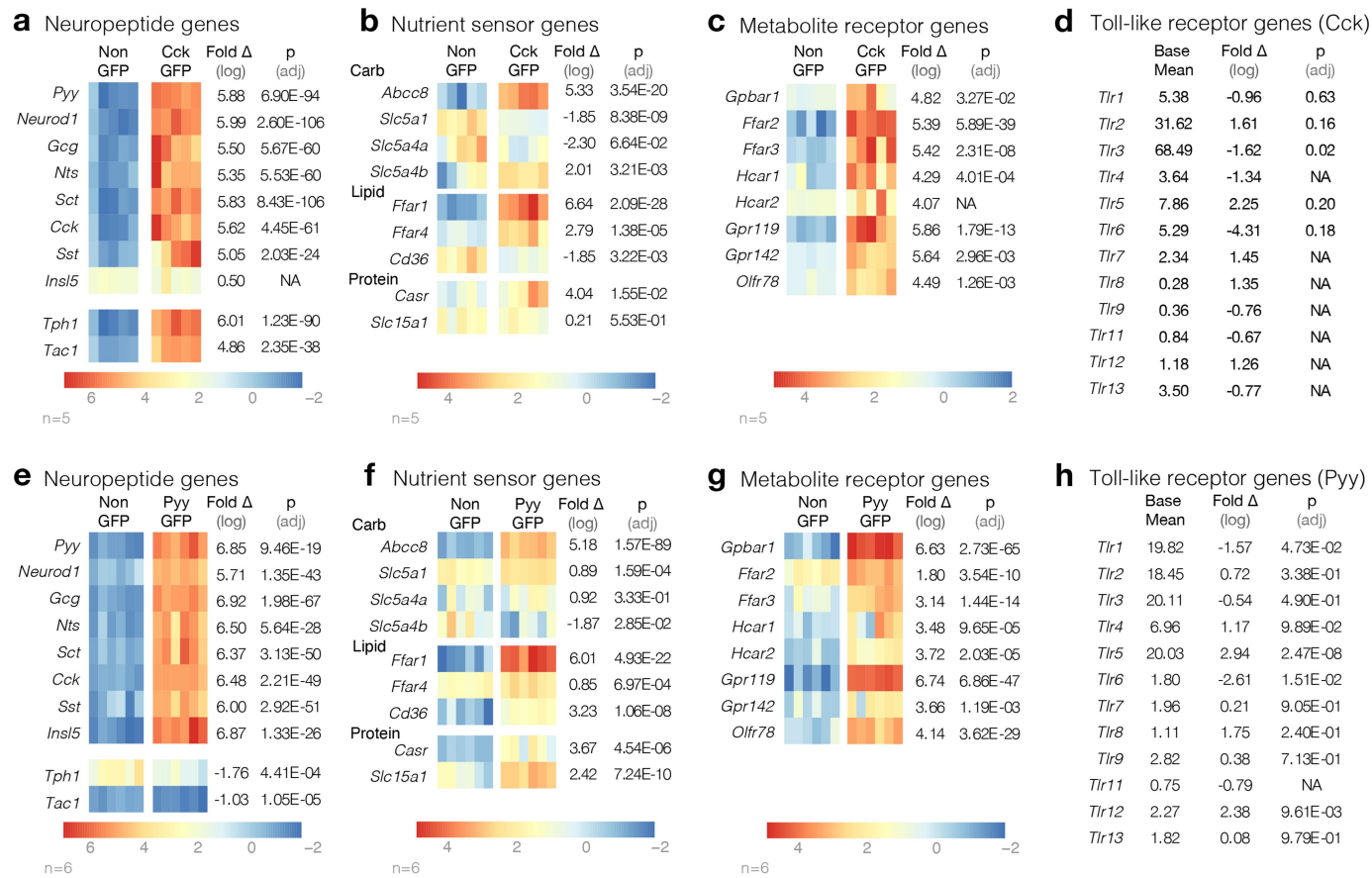
Additional information

Supplementary information The online version contains supplementary material available at <https://doi.org/10.1038/s41586-025-09301-7>.

Correspondence and requests for materials should be addressed to M. Maya Kaelberer or Diego V. Bohórquez.

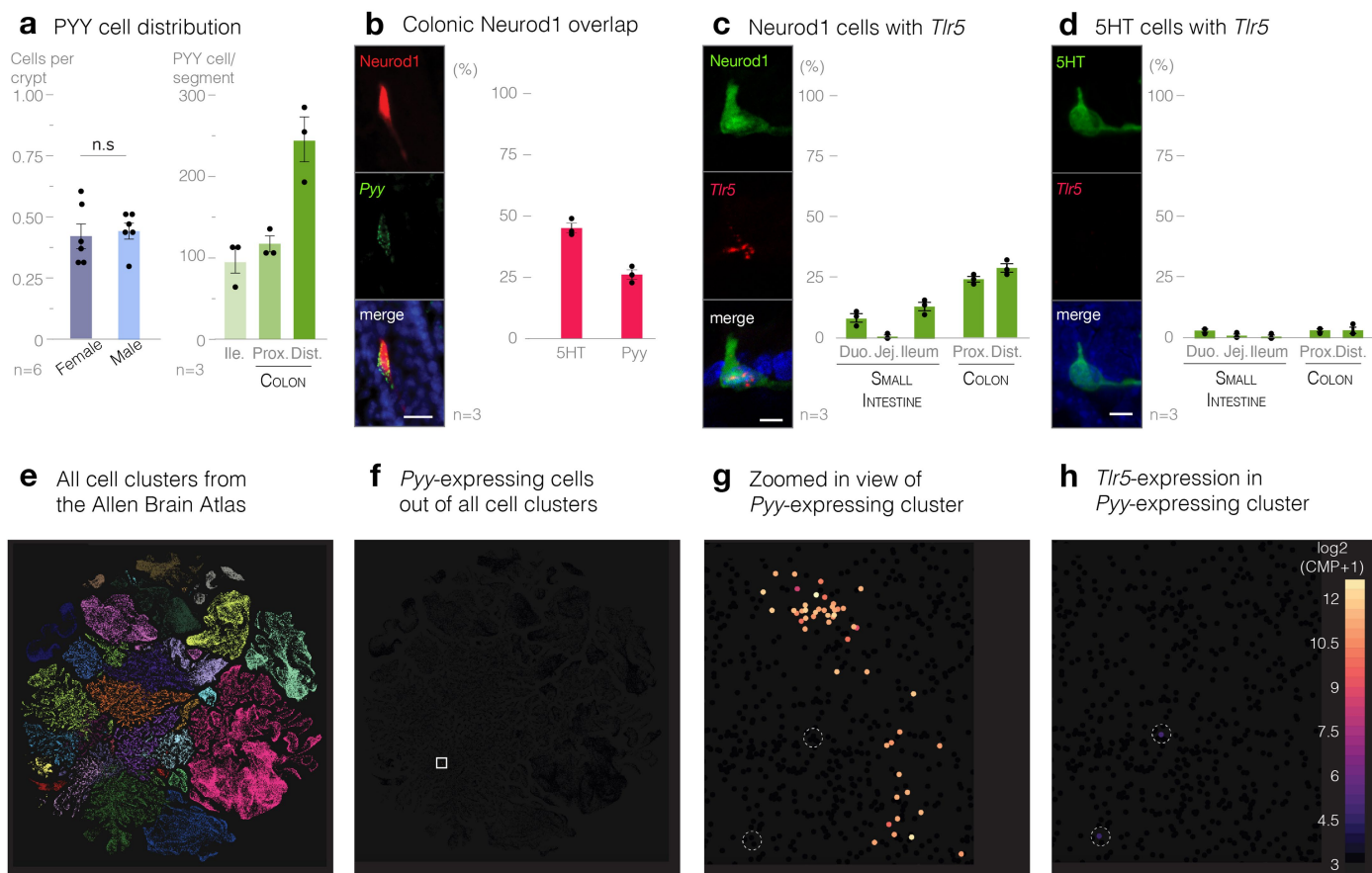
Peer review information Nature thanks John Lukens and the other, anonymous, reviewer(s) for their contribution to the peer review of this work.

Reprints and permissions information is available at <http://www.nature.com/reprints>.



Extended Data Fig. 1 | RNASeq of Cck- and Pyy-labeled cells. Heatmap showing expression of (a,e) neuropeptide, (b,f) nutrient sensor, and (c,g) metabolite receptor genes in non-GFP and CckGFP epithelial cells from the proximal half of the (a-d) small intestine or non-GFP and PyyGFP epithelial cells from the

(e-h) ileum and colon ($n \geq 5$ mice; adjusted P values by DESeq2 with two-tailed t -tests). (d,h) Table of base mean expression, fold change, and adjusted P value of Toll-like receptors between (d) CckGFP cells and non GFP cells and (h) PyyGFP cells and non-GFP cells.

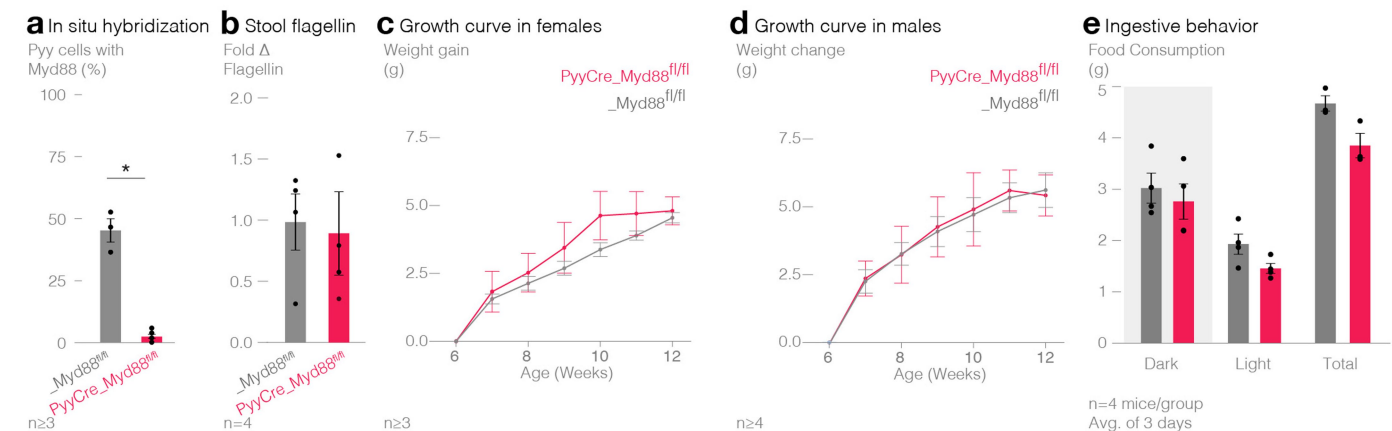


Extended Data Fig. 2 | *Tlr5* transcripts in neuropod cells. (a) (Left) Pyy-labeled neuropod cells per crypt: This panel shows the number of Pyy-positive cells per crypt in female and male mice. Each dot represents the average of 50 crypts analyzed. $P > 0.05$ by two-tailed t-test. (Right) Ileal and colonic tissues from PyyGFP mice ($n = 3$ mice) were evaluated for Pyy cell quantities per segment. (b) (Left) Neurod1Cre_tdTomato (red) cell with ISH labeling of Pyy, representative of $n = 3$ mice. (Right) Quantification of overlap between Neurod1Cre_tdTomato cells with 5HT and Pyy in the colon ($n = 3$ mice, each dot represents $n = 50$ cells). (c) (Left) Neurod1Cre_tdTomato (green) cell with ISH labeling of *Tlr5* (red),

representative of $n = 3$ mice. (Right) Regional expression of *Tlr5* in Neurod1-labeled neuropod cells ($n = 3$ mice, each dot represents $n = 50$ cells). (d) (Left) Antibody-labeled serotonin (green) cell with ISH labeling of *Tlr5* (red), representative of $n = 3$ mice. (Right) Regional expression of *Tlr5* in 5HT cells ($n = 3$ mice, each dot represents $n = 50$ cells). Scale bars = 10 μ m. Error bars represent S.E.M. e-h: Single-cell RNA sequencing (scRNAseq) analysis of whole mouse brain⁴⁶ (Allen Institute Brain Atlas). (f,g) Cluster of Pyy-labeled cells in the medulla. (g,h) These Pyy-labeled cells do not express *Tlr5*. e-h, adapted from ref. 46, Springer Nature Limited, under a Creative Commons licence CC BY 4.0.

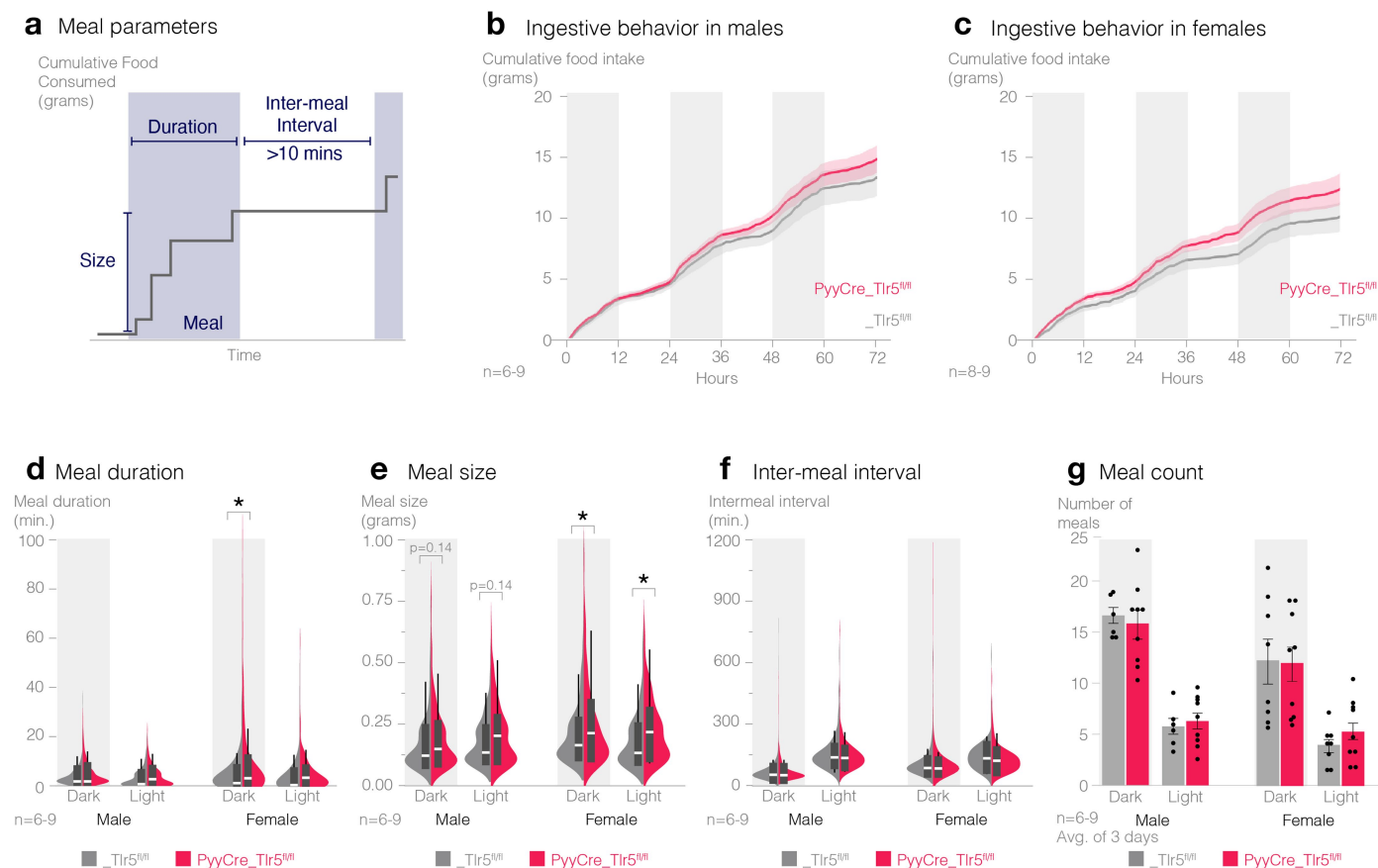
Extended Data Fig. 3 | Metabolic and immune phenotype of PyyCre_Tlr5^{fl/fl} mice. (a) *In-situ* hybridization of *Tlr5* transcripts in colonic Pyy-labeled cells in PyyCre_Tlr5^{fl/fl} mice and _Tlr5^{fl/fl} littermates ($n = 3$ mice per genotype; two-tailed unpaired t-test $*P < 0.05$). Scale bar=10 μ m. Genetic deletion of *Tlr5* in Pyy-labeled cells did not affect (b) oral glucose tolerance, (c) fasting blood glucose, (d) fat pad weights, (e) serum PYY or GLP-1 levels (fasted overnight, one-hour refed), (f) colon length, and (g) weight, or (h) spleen weight ($P > 0.05$ by ANOVA, for sample sizes see Supplementary Table 2). (i) Colonic myeloperoxidase levels ($n = 6$ mice per genotype) and fecal lipocalin-2 levels ($n = 5$ mice per genotype) across genotypes ($P > 0.05$ by two-tailed unpaired t-test). (j) Morpho-pathological analysis of Hematoxylin & Eosin-stained colon sections from PyyCre_Tlr5^{fl/fl} mice and _Tlr5^{fl/fl} control littermates. Proinflammatory lamina propria cells in both groups were within normal limits, representative of $n = 3$ mice. Scale bar=100 μ m. Comparison of colons from PyyCre_Tlr5^{fl/fl} mice and _Tlr5^{fl/fl}

control littermates showed no change in (k) crypt depth ($n = 3$ mice), (l) PYY and 5-HT cell density ($n = 3$ mice), (m) epithelial *Tlr* expression ($n = 6$ mice), or (n) tight junction expression ($n = 6$ mice) ($P > 0.05$ by two-tailed unpaired t-test). (o) Genetic deletion of *Tlr5* in Pyy-labeled cells significantly increased weight gain in males and females (males: $n = 7$ mice for PyyCre_Tlr5^{fl/fl}, $n = 15$ mice for _Tlr5^{fl/fl} littermate controls; females: $n = 6$ mice for PyyCre_Tlr5^{fl/fl}, $n = 11$ mice for _Tlr5^{fl/fl} littermate controls; $*P < 0.05$ genotype*time interaction per sex by rmANOVA with post-hoc two-tailed Tukey HSD). (p) 24 h food consumption was significantly higher in PyyCre_Tlr5^{fl/fl} mice compared to _Tlr5^{fl/fl} littermate controls (males: $n = 4$ mice for PyyCre_Tlr5^{fl/fl}, $n = 7$ mice for _Tlr5^{fl/fl} littermate controls; females: $n = 4$ mice for PyyCre_Tlr5^{fl/fl}, $n = 4$ mice for _Tlr5^{fl/fl} littermate controls; $*P < 0.05$, genotype main effect by ANOVA with post-hoc two-tailed Tukey HSD, no significant differences between days, intake averaged across 3 consecutive days at 21 weeks of age). Error bars represent S.E.M.



Extended Data Fig. 4 | Phenotype of *PyyCre_Myd88^{fl/fl}* mice. (a) In situ hybridization validating the lack of *Myd88* transcripts in colonic Pyy-labeled cells in *PyyCre_Myd88^{fl/fl}* mice ($n = 3, 4$ mice; * $P < 0.05$ by two-tailed unpaired t-test). (b) Genetic deletion of *Myd88* exclusively in Pyy-labeled cells caused no significant change in the relative concentration of flagellin in the stool ($n = 4$ mice, $P > 0.05$ by two-tailed unpaired t-test). *PyyCre_Myd88^{fl/fl}* mice had no changes

in weight gain compared to their littermate controls in both (c) females (*PyyCre_Myd88^{fl/fl}*; $n = 3$ mice, *_Myd88^{fl/fl}*; $n = 4$ mice; $P > 0.05$ by rmANOVA) and (d) males (*PyyCre_Myd88^{fl/fl}*; $n = 4$ mice, *_Myd88^{fl/fl}*; $n = 7$ mice; $P > 0.05$ by rmANOVA). (e) *PyyCre_Myd88^{fl/fl}* had no changes in 24-hour food consumption averaged across 3 consecutive days ($n = 4$ mice; $P > 0.05$ by ANOVA). Error bars represent S.E.M.

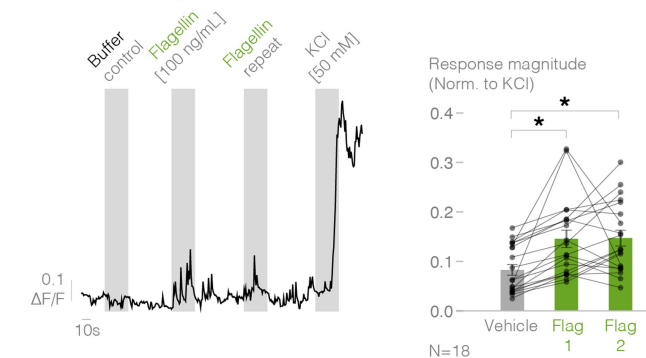


Extended Data Fig. 5 | Meal pattern analysis in PyyCre_Tlr5^{fl/fl} mice.

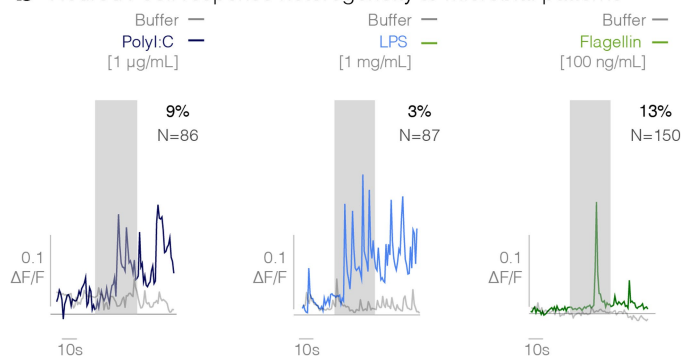
(a) Schematic of meal pattern analysis showing that meals are defined as consumption >0.1 g with at least 10 min in between bouts. Cumulative food consumption was assessed for PyyCre_Tlr5^{fl/fl} and _Tlr5^{fl/fl} littermate control mice across 3 days in the TSE Phenomaster for (b) male and (c) female mice. Quantification of meals across 72 h in the dark and light cycles in males and

females of (d) meal duration, (e) meal size, and (f) inter-meal interval. Box plots represent interquartile range, white lines indicate median, and (g) meal count (PyyCre_Tlr5^{fl/fl}: $n = 9$ male mice and $n = 9$ female mice; _Tlr5^{fl/fl}: $n = 6$ male mice and $n = 8$ female mice; * $P < 0.05$ genotype main effect by ANOVA with post-hoc two-tailed Tukey HSD).

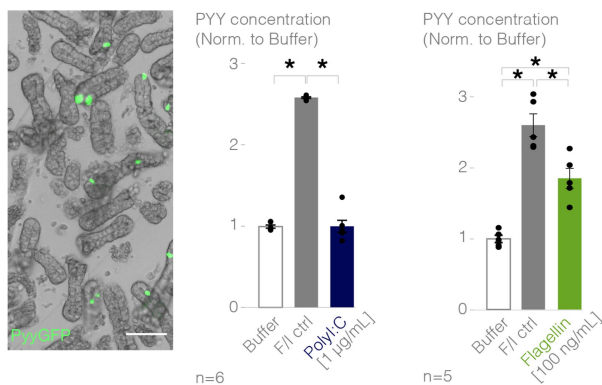
a Calcium imaging in colonic Neurod1_Salsa6f cells



b Neurod1 cell response heterogeneity to microbial patterns



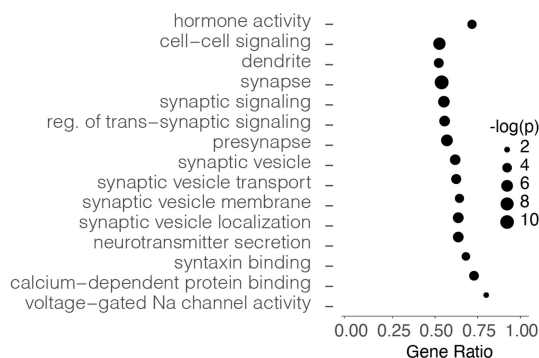
c PYY release assay in colonic epithelia



Extended Data Fig. 6 | Enteroendocrine cells are activated by flagellin.

(a) (Left) Selected Calcium trace from acutely dissociated Neurod1Cre_Salsa6f colonic cells demonstrating experimental paradigm, representative of $n = 18$ cells. Each cell was exposed to each stimulus twice, and a responder was defined as a cell that responded twice. (Right) Quantification of calcium response magnitude of flagellin responders ($*P < 0.05$ by rmANOVA with post-hoc two-tailed Tukey HSD). (b) Calcium traces from acutely dissociated Neurod1Cre_Salsa6f colonic cells. 9% of cells responded to 1 $\mu\text{g/mL}$ PolyI:C ($n = 63$ cells, $n = 4$ mice), 3% of cells responded to 1 mg/mL lipopolysaccharide (LPS) ($n = 80$ cells, $n = 4$ mice), and 13% of cells responded to 100 ng/mL flagellin ($n = 121$ cells, $n = 6$ mice). Gray indicates 30 s infusion. (c) (Left) Immunofluorescence image showing plated colonic crypts with individual Pyy-labeled cells (green) in PyyGFP mice. Scale bar=10 μm . (Middle) Stimulation of colonic crypts with cAMP activators 1 μM forskolin and 10 μM IBMX, but not 1 $\mu\text{g/mL}$ PolyI:C induce PYY release ($n = 6$ mice). (Right) Stimulation of colonic crypts with cAMP activators 1 μM forskolin and 10 μM IBMX, and 100 ng/mL flagellin induce PYY release ($n = 5$ mice); $*P < 0.05$ by one way ANOVA with post-hoc Tukey HSD). Error bars indicate S.E.M.

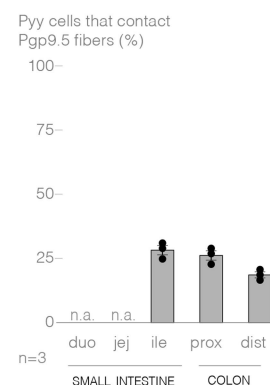
a Gene ontology analysis



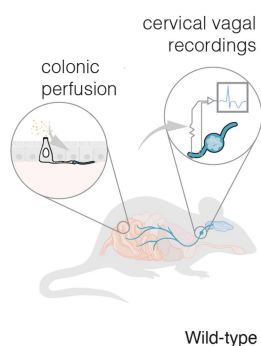
b Pre-synaptic genes

	Base Mean	Fold Δ (log)	p-value (adj)
Cplx2	401.75	-5.04	2.50E-85
Cacna1a	114.88	-3.49	7.84E-70
Pclo	155.99	-3.99	4.89E-39
Sv2a	34.53	-3.45	1.20E-13
Syn1	121.20	-1.58	1.92E-08
Syp	60.79	-3.08	1.79E-23
Syt7	123.57	-2.49	1.91E-19
Syt14	36.72	-2.99	1.07E-07
Stx1a	51.27	-4.27	2.53E-44
Vamp4	173.79	-1.54	1.62E-14
Nrxn1	285.75	-2.71	5.90E-24

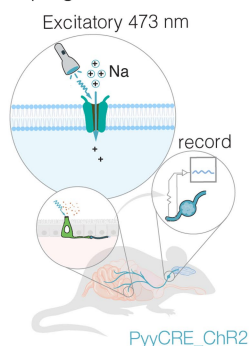
c Contacts with nerves



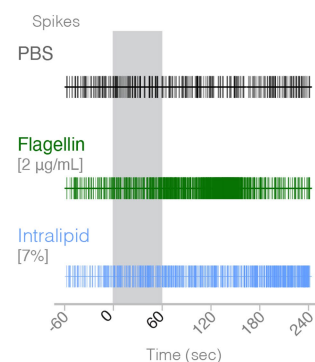
d Vagal recording schematic



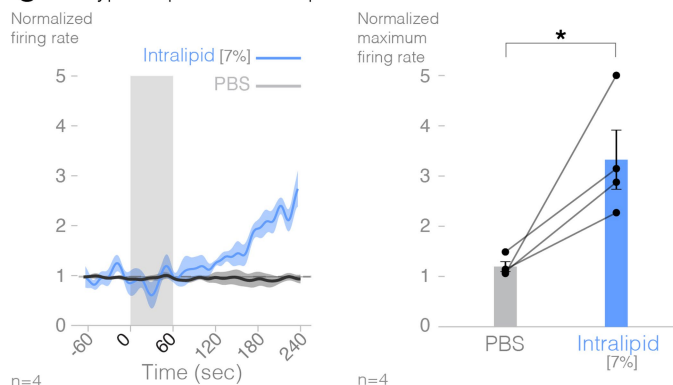
e Optogenetic activation



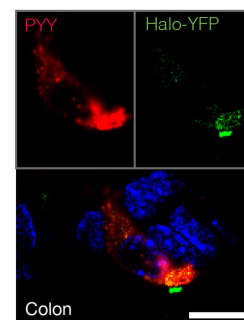
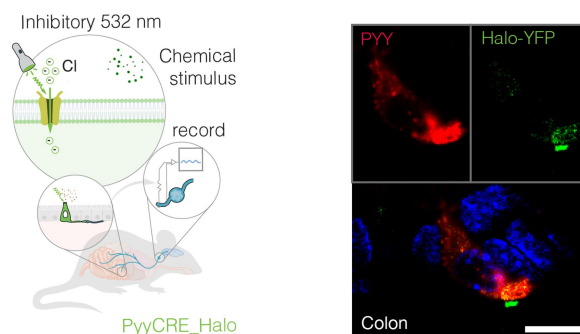
f Vagal firing with colonic infusion



g Wildtype response to intralipid

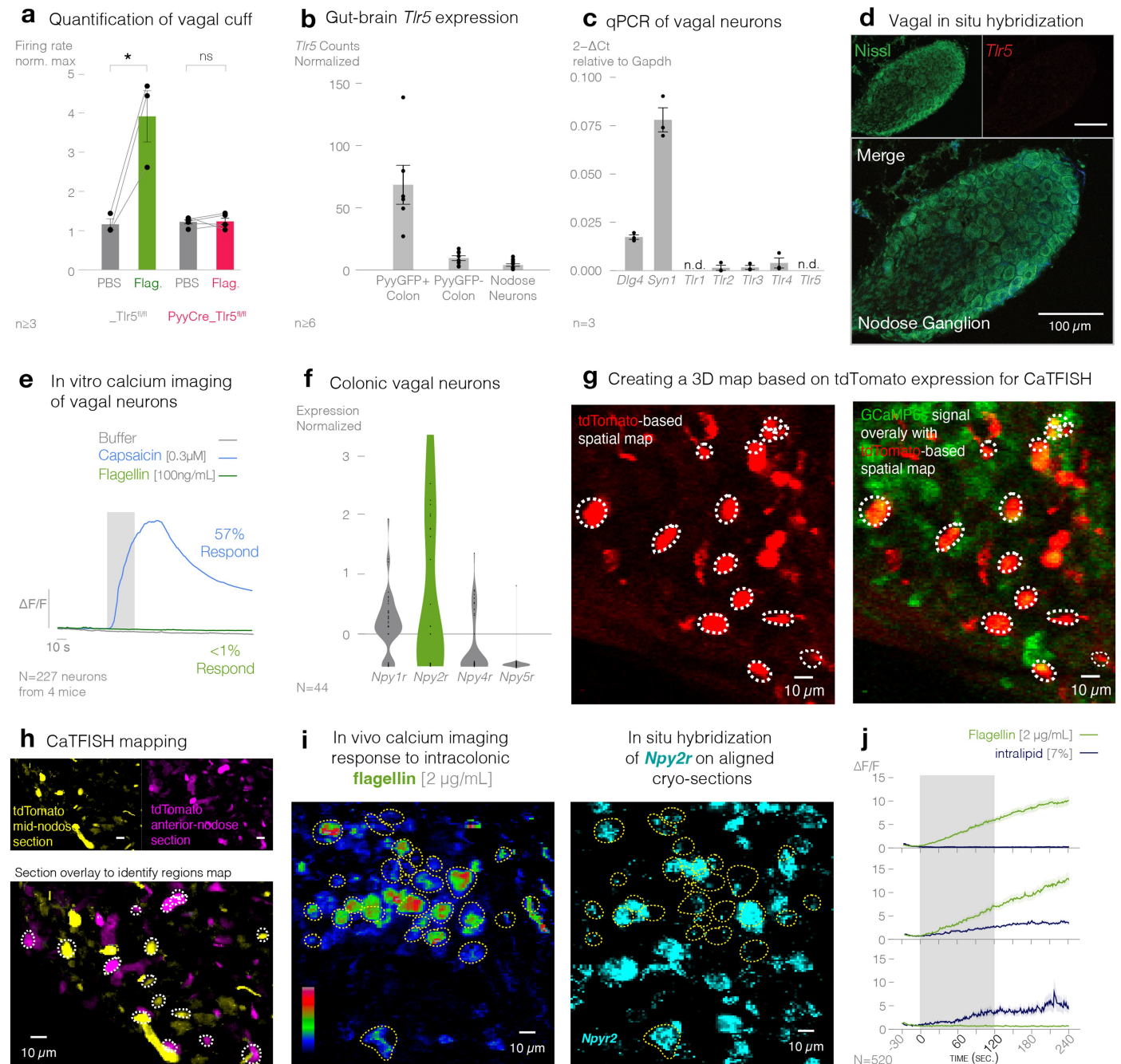


h Optogenetic inhibition



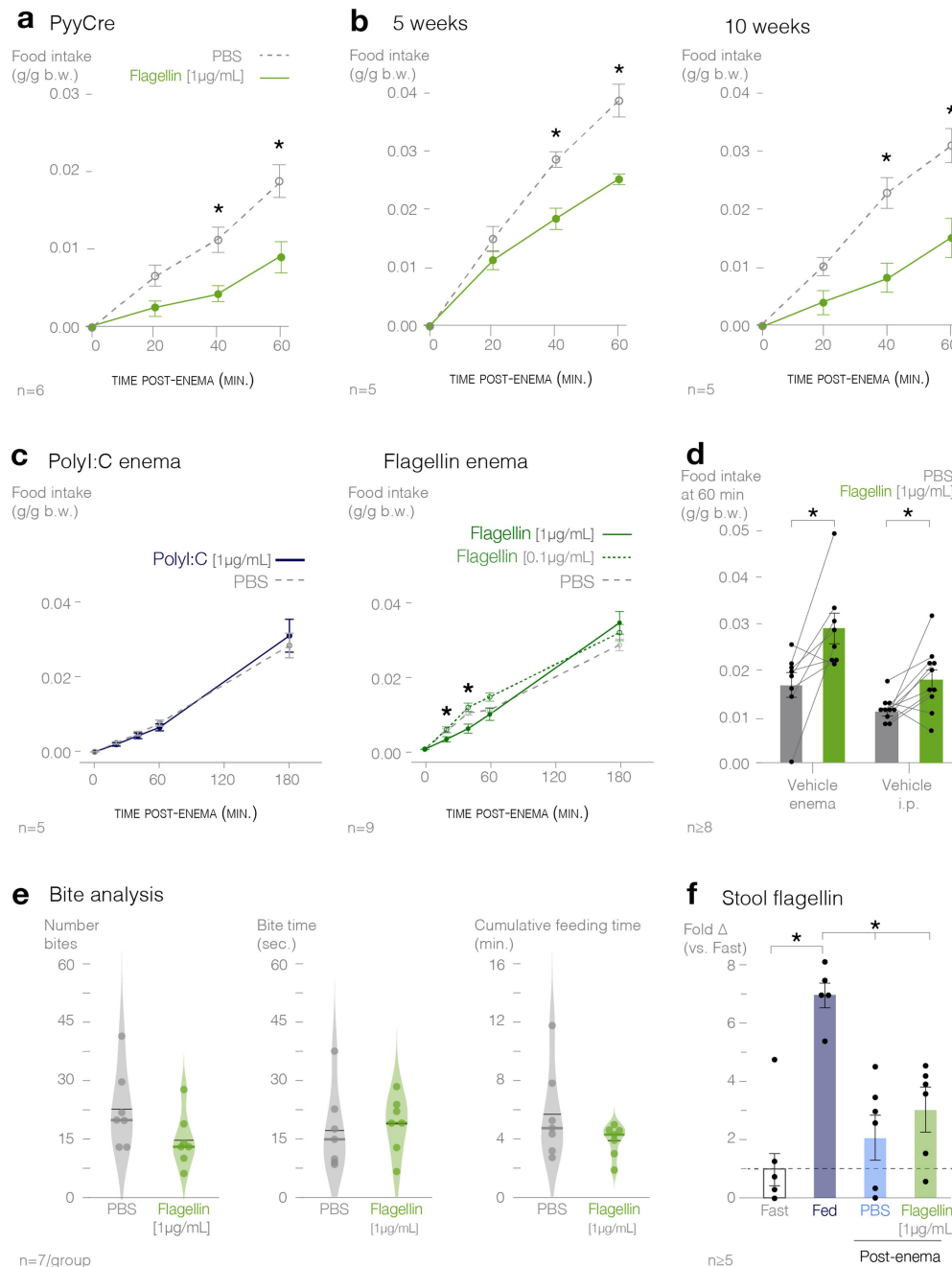
Extended Data Fig. 7 | Vagal neurons are contacted by Pyy-labeled cells and are activated by intracolonic stimuli. (a) List of significantly enriched gene ontology terms related to neuronal connection in Pyy-labeled cells ($n = 6$ mice; adjusted $*P < 0.05$ by topGO analysis). (b) Table of base mean, fold change, and adjusted P value for pre-synaptic genes between PyyGFP cells and non-GFP cells (DESeq2 with two-tailed t-tests). (c) Quantification of contacts between Pyy-labeled cells and Pgp9.5 neuronal fibers in different regions of the intestine ($n = 3$ mice). (d) Schematic of the vagal recording technique. The cervical vagus was recorded while the entire colon was simultaneously perfused with stimulus. (e) (Left) Schematic demonstrating 473 nm light via an intracolonic light emitting diode (LED) activating the cation channel Channelrhodopsin (ChR2) and depolarizing a Pyy-labeled cell. (Right) Representative image showing expression

of ChR2-tdTomato (red) in a colonic Pyy-labeled cell (green). (f) Spike raster from vagal recordings in which PBS, 2 µg/mL flagellin, or 7% intralipid was perfused into the colon, representative of $n = 4$ mice. Gray bar represents the perfusion interval. (g) (Left) Vagal responses to intracolonic perfusion of PBS or 7% intralipid in wild-type mice ($n = 4$ mice). Error bars indicate S.E.M. (Right) Quantification of peak response to intralipid ($*P < 0.05$ by two-tailed paired t-test). (h) (Left) Schematic demonstrating 532 nm light activating the anion channel Halorhodopsin (Halo) and hyperpolarizing a Pyy-labeled cell. (Right) Representative image showing expression of Halorhodopsin-YFP (Green) in a colonic Ppy-labeled cell (red). Scale bars=10µm. Graphics in d,e,h adapted from ref. 3, AAAS.



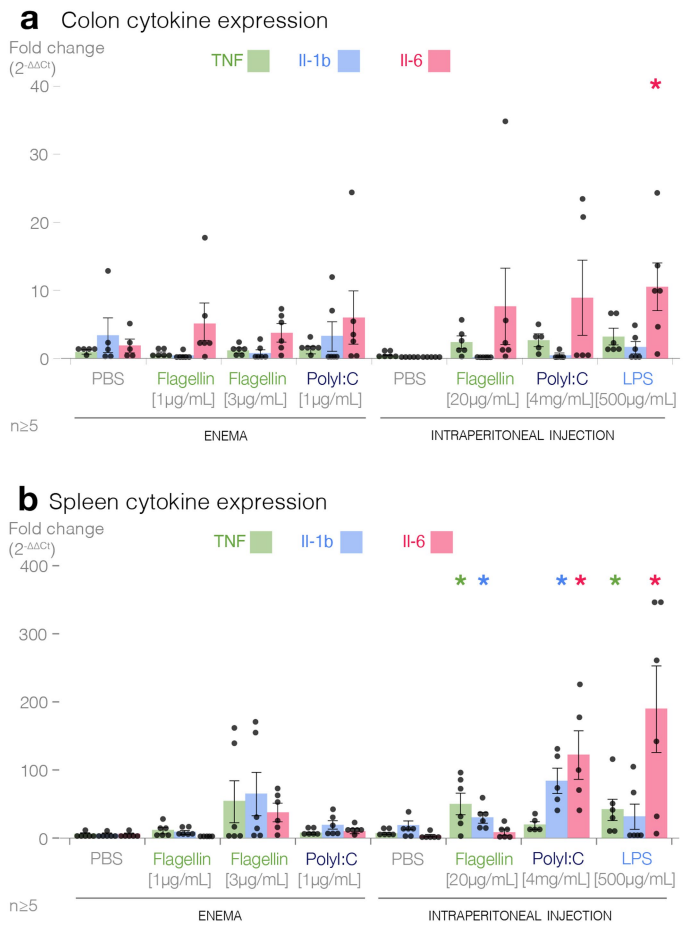
Extended Data Fig. 8 | Vagal neurons neither express *Tlr5* nor respond directly to flagellin. (a) Quantification of the peak vagal response to flagellin in *PyyCre_Tlr5^{fl/fl}* and *_Tlr5^{fl/fl}* littermate controls (*PyyCre_Tlr5^{fl/fl}*; $n = 5$ mice; *_Tlr5^{fl/fl}*; $n = 3$ mice; $*P < 0.05$ by Kruskal Wallis test with non-parametric comparisons using the Wilcoxon method). (b) RNAseq of vagal nodose neurons showed no expression of *Tlr5* (*PyyGFP+* cells; $n = 5$ mice, *PyyGFP-* cells; $n = 8$ mice, nodose neurons; $n = 8$ mice; DESeq2 normalization). (c) qPCR of synaptic markers and Toll-like receptors in vagal nodose neurons ($n = 3$ mice). (d) In situ hybridization of Nissl (green) stained neurons of the nodose ganglion showed no expression of *Tlr5* (red), representative of $n = 3$ mice. Scale bars=100 μm . (e) Representative trace of calcium transient in acutely dissociated NeuroD1Cre-Salsa6f nodose neurons showed responses in 57% of neurons to capsaicin, but

not to flagellin ($n = 227$ neurons, $n = 4$ mice). (f) Secondary analysis of data from Bai et al., 2018 of the colon-projecting vagal neurons showed expression of the PYY receptor *Npy2r* ($n = 44$ cells). (g) Spatial overlay of vagal nodose neurons using tdTomato and GCaMP6s fluorescence. (h) Spatial overlay of vagal nodose neurons using compartment analysis of temporal activity by fluorescence in situ hybridization (CaTFISH). (i) Representative image of CaTFISH mapping of in vivo calcium transients onto *Npy2r* positive neurons. Scale bars=10 μm . (j) Calcium traces from vagal nodose neurons responsive to either only flagellin (2 $\mu g/mL$) (top), intralipid (7%) and flagellin (2 $\mu g/mL$) infused separately (middle), or only intralipid (7%) (bottom), representative of $n = 520$ neurons. Error bars and shades indicate S.E.M. **f**, adapted from ref. 56, Cell Press.



Extended Data Fig. 9 | Intracolonic flagellin modulates food intake. Mice were fasted overnight and received flagellin (1 μ g/mL) or PBS enemas prior to gaining ad libitum access to standard chow for 60 min. Flagellin reduced food intake compared to PBS in (a) PpyCre mice ($n = 6$ mice); (b) 5-week-old mice ($n = 5$ mice); and 10-week-old mice ($n = 5$ mice; $*P < 0.05$, enema*time interaction by rmANOVA with post-hoc two-tailed Tukey HSD). (c) (Left) Polyl:C (1 μ g/mL) enema was not sufficient to alter food intake compared to PBS enema ($n = 5$ mice; $P < 0.05$, enema*time interaction by rmANOVA with post-hoc two-tailed Tukey HSD). (Right) Effects of flagellin dissipated after 180-minutes post-enema ($n = 9$ mice; $P > 0.05$ at 180 min by post-hoc Tukey HSD). (d) Neither vehicle enema (dimethyl sulfoxide, DMSO; $n = 8$ mice) nor vehicle intraperitoneal injection (saline; $n = 10$ mice) altered feeding response to flagellin enema

($P < 0.05$ by two-tailed t-test). (e) Crunch Master analysis of bites for number of bites, bite time, which is the average time of a single feeding bout, and feeding time which is the number of minutes that mice engaged in feeding, did not change during the 1-hour recording session ($n = 7$ mice per treatment group; $P > 0.05$ by two-tailed unpaired t-test). Violin plots show median indicated by thick line and mean indicated by thin line. (f) Relative flagellin concentration was measured in stool collected from wildtype mice following an 18-hour fast ($n = 5$ mice), ad libitum feeding ($n = 5$ mice), or an 18-hour fast plus enema of PBS ($n = 6$ mice) or flagellin [1 μ g/mL] ($n = 6$ mice). Feeding significantly increased stool flagellin, however, flagellin enema was not sufficient to rescue flagellin levels to the fed state ($*P < 0.05$ by rmANOVA with post-hoc two-tailed Tukey HSD). Error bars indicate S.E.M.



Extended Data Fig. 10 | Flagellin enema is not sufficient to induce an immune response. (a) Cytokine expression in the colon 1 h after enema of PBS ($n = 5$ mice), flagellin [1 µg/mL] ($n = 6$ mice), flagellin [3 µg/mL] ($n = 6$ mice), PolyI:C [1 µg/mL] ($n = 6$ mice), or intraperitoneal (i.p.) injection of PBS ($n = 6$ mice), flagellin [20 µg/mL] ($n = 6$ mice), PolyI:C [4 mg/mL] ($n = 5$ mice), LPS [500 µg/mL] ($n = 6$ mice) ($*P < 0.05$ significance from PBS enema group by non-parametric two-tailed Wilcoxon each pair test). (b) Cytokine expression in the spleen 1 h after enema of PBS ($n = 6$ mice), flagellin [1 µg/mL] ($n = 6$ mice), flagellin [3 µg/mL] ($n = 6$ mice), PolyI:C [1 µg/mL] ($n = 6$ mice), or intraperitoneal (i.p.) injection of PBS ($n = 6$ mice), flagellin [20 µg/mL] ($n = 6$ mice), PolyI:C [4 mg/mL] ($n = 5$ mice), LPS [500 µg/mL] ($n = 6$ mice) ($*P < 0.05$ significance from PBS enema group by non-parametric two-tailed Wilcoxon each pair test). Error bars indicate S.E.M.